Korean J. Chem. Eng., 39(2), 284-305 (2022)
DOI: 10.1007/s11814-021-0939-5

pISSN: 0256-1115
eISSN: 1975-7220

Combinatorial and geometric optimization of a parabolic trough solar collector

Anubhav Goel*, Gaurav Manik*,†, and Om Prakash Verma**

*Department of Polymer and Process Engineering, Indian Institute of Technology Roorkee, India
**Department of Instrumentation and Control Engineering, Dr. B R Ambedkar National Institute of Technology Jalandhar, India
(*Received 30 May 2021 • Revised 25 July 2021 • Accepted 24 August 2021*)

Abstract−The current investigation reveals the need for combinatorial and geometric optimization for parabolic trough solar collectors (PTSCs) and proposes methods to perform them. An analytical model of PTSC was drafted, which emerged to be quite accurate when exhaustively validated using experimental results. The analysis reveals that superior properties of design components (solar selective absorber coatings (SSACs), heat transfer fluids (HTFs), etc.) cannot guarantee better performance, as there are many interacting factors. Also, a particular combination of components can perform better at a certain temperature while lagging at another. To acquire an optimal combination of components, combinatorial optimization is introduced and carried out for PTSCs, using genetic algorithm (GA). Six SSACs, three absorber materials, and five HTFs are considered, significant efficiency improvements of 8% at 150 °C and 6% at 300 °C are observed. This study discloses that geometrical parameters (length and width of collector, focal length, etc.) possess positive as well negative impacts on efficiency. By varying these in a reasonable range, optimal values that lead to improved efficiency can be obtained. Particle swarm optimization (PSO) is used to attain this geometric optimization, and improvement of ≥3% in efficiency is noticed by only ±5% variation in dimensions.

Keywords: Parabolic Trough Solar Collector, Analytical Modeling, Geometric Optimization, Combinatorial Optimization, Particle Swarm Optimization, Genetic Algorithm

INTRODUCTION

The need to control and minimize the current reliance on hazardous energy sources is eminent. The direct use of solar radiation to generate heat has shown great potential to gradually replace fossil fuels in different spheres like power generation, desalination, process heat in industries, and others [1]. The parabolic trough solar collector (PTSC) is among the pioneering approaches. It can convert solar energy to thermal energy and has already shown excellent proficiency in power generation sector. PTSCs also have promising potential to serve industrial process heat (IPH) applications, requiring working temperatures in the range of 50-260 °C [2]. The practical realization of the same is still in progress.

Many processes in industries require heat energy, like pre-heating, drying and degreasing, curing, sterilization, and others [3]. All these processes have different needs in terms of temperature and working medium, some need heated air for drying, some require steam and so on [4,5]. Accordingly, PTSC has to fulfill the specific needs of an IPH application and it will be beneficial if a PTSC with maximized performance is employed for the same. To accomplish this, it is vital to deal with several working parameters that affect the performance of PTSC. Such parameters include absorber material, optical properties of materials used, type of working fluid, shape of collector, type of tracking system, reflector material [6]. Besides these, the dimensions of each component of PTSC can alter the efficiency. Thus, to serve a specific industrial process, it becomes necessary to estimate an optimal set of parameters and dimensions for a PTSC. Such a collection of parameters can be obtained by utilizing the optimization techniques.

Many studies have employed optimization techniques in the recent past for optimization purposes in context with PTSCs. Ajbar et al. [7] worked on inverting artificial neural network (ANN) models that yielded a multivariable objective function. They further solved the problem using genetic algorithm (GA) and particle swarm optimization (PSO) to determine optimal input variables. A multi-objective optimization of the system using PTSCs to operate the screw expander-based cascade Rankine cycle was earlier conducted by Habibi et al. [8] via GA. The least squares support vector machine (LSSVM) method was employed by Liu et al. [9] to model the PTSC. The relationship between PTSC efficiency and various parameters was extracted for two different solar fields. Zadeh et al. [10] used two different thermo-physical models for nanofluid modeling. Subsequently, the thermal performance was improved using hybrid optimization algorithm comprising GA and sequential quadratic programming (GA-SQP). ANN models were utilized by Boukelia et al. [11] for techno-economic optimization of PTSC based thermal power plants. Thermo-economic optimization of parabolic trough solar plant was pursued by Silva et al. [12]. The number of troughs in series or parallel, row spacing, and energy storage volume were considered as design variables and optimized using memetic algorithms.

Genetic algorithm-back propagation (GA-BP) neural network model was used by Wang et al. [13] to optimize absorber output energy, thermal efficiency, and heat loss. Tzuc et al. [14] trained a feed-forward neural network using the experimental database in their work to determine the optimal operating conditions for a

†To whom correspondence should be addressed.
E-mail: gaurav.manik@pe.iitr.ac.in
Copyright by The Korean Institute of Chemical Engineers.

PTSC. Multi-objective optimization of PTSC based tri-generation system was done by Bellos et al. [15] under the steady-state conditions with different criteria. Exergoeconomic optimization of commercial PTSC was proposed by Hoseinzadeh et al. [16] and a hybrid algorithm involving GA and PSO was used. Ehyaei et al. [17] earlier performed the optimization for PTSCs using multi-objective PSO while varying geometric specifications and flow rate. Cheng et al. [18] performed geometric optimization using PSO and Monte Carlo ray-tracing method to improve the optical performance of PTSC.

It is evident from the previous studies that optimization can play an important role in the analysis and development of PTSCs. Most of the studies are noticed to be concerning the use of PTSC in power generation, and accordingly, the parameters related to it were optimized. Mostly nature-inspired algorithms have been applied, which is expected here as the performance estimations in PTSC involve many nonlinear functions.

Operation of PTSC is influenced by components such as solar selective absorber coating (SSAC), heat transfer fluid (HTF), and absorber material. A combination of these design elements can influence the PTSC efficiency as they come in a variety of types with diverse properties. The current work investigated the effect of changing the type of design components of PTSC over its thermal efficiency. Consequently, it helps to optimize them in an attempt to project the use of PTSC in IPH applications. As per the knowledge and beliefs of authors, this study proposes and analyses, for the first time, the concept and importance of combinatorial optimization for PTSCs. Further, the impact of variations in geometric properties (length, width, etc.) of PTSC over its efficiency was also examined first time extensively in this work, and accordingly, geometric optimization was carried out.

The contribution of this work is as follows:

- An improved analytical model of PTSC is presented and thoroughly validated.
- A sensitivity analysis demonstrates the effect of variation in geometric parameters and type of design components for PTSC over its efficiency.
- Unveils the need for geometric and combinatorial optimization for PTSC.
- Combinatorial and geometric optimization are conducted using the meta-heuristic approaches: Genetic algorithm (GA) and Particle Swarm Optimization (PSO).

Moreover, the effect of various governing operators of PSO on the current optimization problem is addressed. The reasons for choosing PSO and GA for optimizations are discussed in respective sections. The improvements in efficiency with optimal parameters and how this can help to push the usage of PTSCs in IPH applications are also discussed.

This paper is organized as follows: Section 2 gives an overview of the components of PTSC and summarizes the development of its analytical model. Essential details for validation of the model are included in Section 3. Section 4 comprises the validation results, sensitivity analysis of PTSC, and results obtained by optimization and discusses them elaborately, while Section 5 sums up the critical results of this work.

MATHEMATICAL MODELING OF PTSC

1. PTSC Description

PTSC can be termed as a line focusing collector that concentrates and converts solar energy into usable heat energy. It is composed of various components having essential properties designed to execute specific tasks for making it operational. It has a parabolic-shaped reflective mirror that converges the solar radiation falling on its surface to the heat collection element (HCE) set at its focal line. An HCE is composed of a metal tube (absorber) with its outer surface coated with a solar selective absorber coating (SSAC) and a glass tube as an envelope. The annulus space between the two is evacuated and glass-to-metal seals are provided at each end of the absorber to account for differential thermal expansion. Evacuation helps to maintain the absorber's performance by protecting it from oxidation and reducing heat losses. Heat transfer fluid (HTF), such as water, thermic oil, or some organic solvent, flows through the absorber and gains heat energy. The obtained energy can be utilized to serve different applications. A better conception of these can be attained by looking at Fig. 1.

2. Optical Analysis

Solar radiation reaching the collector is converged towards HCE, where it is absorbed in glass envelope ($Q_{e_o Ab}$) and absorber ($Q_{a_o Ab}$) to initiate the heat transfer mechanisms. Thus, it is necessary to evaluate optical efficiency before evaluating thermal efficiency.

Optical efficiency (η_O) is the ratio between the solar energy ab-

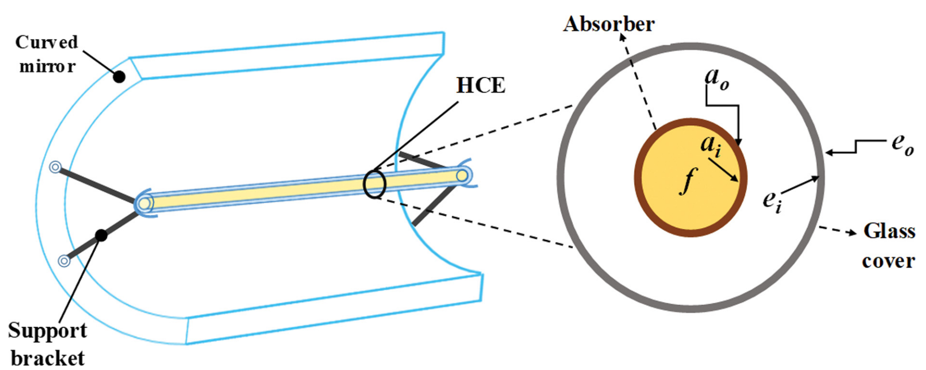

Fig. 1. Illustration of PTSC along with the cross-sectional view of kth segment of its HCE.

sorbed by absorber tube and the solar irradiation received at the glass envelope [19]. It is influenced by various factors, such as [20, 21] geometric error (ε_{ge}), collector reflectivity (∂_r), tracking error (ε_{te}), mirror cleanliness (ε_{dm}), HCE cleanliness (ε_{dhce}), miscellaneous aspects (ε_m), and collector shadowing (ε_{se}).

All the terms mentioned above are effective when the angle of incidence (θ) is zero and are accounted collectively by a term intercept factor ($\gamma_{in}=\varepsilon_{ge}\varepsilon_{te}\varepsilon_{se}\varepsilon_{dm}\varepsilon_{dhce}\varepsilon_m$). If $\theta\neq0$, then the value of γ_{in} introduces errors and need to accommodate one more term known as incident angle modifier (K_θ). To evaluate K_θ, an empirical relation derived through experimental data is used. For different setups analyzed here and emphasized in Section 3, correlations for K_θ are as follows:

$$K_\theta=\cos(\theta)+0.000884\theta-0.00005369\theta^2 \quad \text{for SEGS LS-2 [22]} \tag{1}$$

$$K_\theta=\cos(\theta)+0.0003178\theta-0.00003985\theta^2 \quad \text{for IST PTSC [23]} \tag{2}$$

$$K_\theta=\cos(\theta)-7\times10^{-4}\theta-36\times10^{-6}\theta^2 \quad \text{for HTF test bench [24]} \tag{3}$$

When $\theta\neq0$, one more effect sets in, in which a portion of HCE near its ends is partially illuminated by incident solar beam; this is known as end loss (E_θ). Reasonable estimates of the same can be obtained using the correlation by Lippke [25], given as:

$$E_\theta=1-\left\{\left(\frac{f_{cl}}{l_{cl}}\right)\tan\theta\right\} \tag{4}$$

where, f_{cl} is the focal length and l_{cl} is the collector length for PTSC. Along with the above discussed terms, optical properties of the SSAC and the glass envelope are required to calculate $Q_{e_o Ab}$ and $Q_{a_o Ab}$ as:

$$Q_{e_o Ab}=\eta_{O-e}\alpha_e Q_{sol} \tag{5}$$

$$\eta_{O-e}=\gamma_{in}K_\theta E_\theta \partial_r \tag{6}$$

$$Q_{Sol}=(DNI)A_{cl}/l_{hce} \tag{7}$$

where, η_{O-e} is optical efficiency at glass envelope, A_{cl} is the area of collector, Q_{Sol} is direct normal irradiation (DNI) received per unit length (l_{hce}) of HCE, ∂_r represents the collector reflectivity, and α_e is absorptance of the glass envelope.

$$Q_{a_o Ab}=\eta_{O-ab}\alpha_{ab}Q_{Sol} \tag{8}$$

$$\eta_{O-ab}=\eta_{O-e}\tau_e \tag{9}$$

where, η_{O-ab} represents optical efficiency at absorber surface, τ_e is the transmittance of the glass envelope and α_{ab} is absorptance of the absorber.

3. Thermal Analysis

To examine the performance of HCE, energy balance equations are formulated by considering the energy conservation at each of its cross-sectional surfaces. HCE is axially discretized into N segments and the k^{th} segment is analyzed radially, a sketch of the same is shown in Fig. 1.

It is observed that $Q_{a_o Ab}$ is conducted primarily through absorber cross-section ($Q_{a_o-a_i Cond}$) and is transferred to HTF via convection ($Q_{a_i-f Conv}$). A part of remaining energy goes to annulus through convection ($Q_{a_o-e_i Conv}$) and radiation ($Q_{a_o-e_i Rad}$). Another part conducts to support brackets ($Q_{Brac-Cond}$) and vanishes to the environment.

Energy reaching the inner surface of glass envelope is conducted to its outer surface ($Q_{e_i-e_o Cond}$). This energy, along with the $Q_{e_o Ab}$ perishes to surrounding air by convection ($Q_{e_o-s Conv}$) and to sky by radiation ($Q_{e_o-sky Rad}$). As a whole, the following set of equations is obtained:

$$Q_{a_i-f Conv}=Q_{a_o-a_i Cond} \quad \text{(at } a_i\text{)} \tag{10}$$

$$Q_{a_o Ab}=Q_{a_o-a_i Cond}+Q_{a_o-e_i Conv}+Q_{a_o-e_i Rad}+Q_{Brac-Cond} \quad \text{(at } a_o\text{)} \tag{11}$$

$$Q_{a_o-e_i Conv}+Q_{a_o-e_i Rad}=Q_{e_i-e_o Cond} \quad \text{(at } e_i\text{)} \tag{12}$$

$$Q_{e_i-e_o Cond}+Q_{e_o Ab}=Q_{e_o-s Conv}+Q_{e_o-sky Rad} \quad \text{(at } e_o\text{)} \tag{13}$$

Each heat transfer term mentioned in these equations has its own evaluation method that can be understood by going through the following sub-sections.

3-1. Radiative Heat Transfers

In HCE, radiative heat transfer occurs at two places. First in the annulus region, an analytical expression based on Stefan-Boltzmann Law is used to evaluate this heat transfer and is given as [26]:

$$Q_{a_o-e_i Rad}=\frac{\sigma\pi D_{a_o}(T_{a_o}^4-T_{e_i}^4)}{\left(\frac{1-\varepsilon_{a_o}}{\varepsilon_{a_o}}+\frac{1}{F_{a_o e_i}}+\left(\frac{(1-\varepsilon_e)D_{a_o}}{\varepsilon_e D_{e_i}}\right)\right)} \tag{14}$$

where, ε_{a_o} is the emissivity of SSAC, ε_e is the emissivity of glass envelope, $F_{a_o e_i}$ is view factor and σ is Stefan-Boltzmann constant.

Secondly, the temperature difference between the glass envelope and the sky sets up radiative heat transfer. The expression to evaluate its value is also based on Stefan-Boltzmann Law and is written as [27]:

$$Q_{e_o-sky Rad}=\sigma\varepsilon_e\pi D_{e_o}(T_{e_o}^4-T_{sky}^4) \tag{15}$$

where, T_{sky} is the temperature of the sky whose value is affected by environmental factors and calculated as [28]:

$$T_{sky}=0.0553T_s^{1.5} \tag{16}$$

3-2. Convective Heat Transfers

For the HCE described, convective heat transfer takes place at three different locations, whose estimations are discussed hereafter.

3-2-1. From the Inner Surface of Absorber to HTF

Convective heat transfer is perceived to be proportional to the temperature difference and, by using Newton's law of cooling [29], can be calculated as:

$$Q_{a_i-f Conv}=\pi D_{a_i}h_f(T_{a_i}-T_f) \tag{17}$$

$$h_f=Nu_{D_{a_i}}\frac{k_f}{D_{a_i}} \tag{18}$$

where, k_f is the thermal conductivity of the HTF at T_f, $Nu_{D_{a_i}}$ is the Nusselt number based on D_{a_i}, and h_f is convective heat transfer coefficient at the mean HTF temperature (T_f).

If flow is laminar (Reynolds number, Re<2300), $Nu_{D_{a_i}}$ can be assumed constant with a value of 4.36, as proposed earlier [26]. In general operating conditions, flow is turbulent (Re>2300) and $Nu_{D_{a_i}}$ can be evaluated using the correlation given by Gnielinski [30]:

$$Nu_{D_{a_i}}=\frac{(fr/8)(Re_{D_{a_i}}-1000)Pr_f}{1+12.7\sqrt{fr/8}(Pr_f^{2/3}-1)}\left(\frac{Pr_f}{Pr_{a_i}}\right)^{0.11} \tag{19}$$

This correlation is valid for $0.5<Pr_{Htf}<2000$ and $2300<Re_{D_{a_i}}<5\times10^6$ with reasonable accuracy. Here, Pr_{a_i} and Pr_f are Prandtl numbers evaluated at T_{a_i} and T_f respectively, while $Re_{D_{a_i}}$ is the Reynolds number calculated at D_{a_i}. Moreover, fr is the friction factor at inner surface of absorber calculated by Colebrook's correlation:

$$fr=[1.5635\ln(Re_{D_{a_i}}/7)]^{-2} \tag{20}$$

3-2-2. In the Annulus Region

The pressure across it governs heat transfer in this region; accordingly, convective heat transfer here is possible in two modes described below:

Case1: *Annulus pressure*<0.013 Pa, at such low pressure, heat transfer takes place via molecular conduction, which can be evaluated using the following [27] correlations.

$$Q_{a_o-e_i\,Conv}=\pi D_{a_o} h_{a_o-e_i}(T_{a_o}-T_{e_i}) \tag{21}$$

where, T_{e_i} is the inner surface temperature of glass envelope, T_{a_o} is the outer surface temperature of absorber and $h_{a_o-e_i}$ is the heat transfer coefficient that can be estimated as [31]:

$$h_{a_o-e_i}=\frac{k_g}{\dfrac{D_{a_o}}{2\ln\left(\dfrac{D_{e_i}}{D_{a_o}}\right)}+b\lambda\left(\dfrac{D_{a_o}}{D_{e_i}}+1\right)} \tag{22}$$

In above correlation, D_{a_o} and D_{e_i} are the diameter of absorber outer surface and glass envelope inner surface, respectively, k_g depicts the thermal conductivity of the gas in the annulus, while b is interaction coefficient and λ is mean free path between collisions of molecules of a gas.

Case 2: *Annulus pressure*>0.013 Pa, if the annulus loses vacuum, external air enters and pressure rises; in this situation, heat transfer occurs via natural convection. To estimate it, a method involving the conduction boundary-layer adopted by Kuehn and Goldstein [32] is used as:

$$Q_{a_o-e_i\,Conv}=\pi D_{a_o} h_{a_o-e_i}(T_{a_o}-T_{e_i}) \tag{23}$$

$$h_{a_o-e_i}=Nu_{a_o-e_i}\frac{k_g}{D_{a_o}} \tag{24}$$

where, $Nu_{a_o-e_i}$ is the Nusselt number for overall heat transfer and is evaluated as follows:

$$Nu_{an\_Conv}=\frac{1}{\ln\left[\dfrac{1+2/Nu_{a_o}}{1-2/Nu_{e_i}}\right]} \tag{25}$$

Nu_{an_Conv} is the average Nusselt number for convection; Nu_{a_o} is mean Nusselt number for outer surface of absorber and Nu_{e_i} for the inner surface of glass envelope.

Next, the Nusselt number (Nu_{an_Cond}) applicable to the situation when heat transfer occurs by conduction is calculated.

$$Nu_{an\_Cond}=\frac{1}{\cosh^{-1}[(D_{a_o}^2+D_{e_i}^2-4\xi^2)/2D_{a_o}D_{e_i}]} \tag{26}$$

where, ξ is the perpendicular distance between the axis of the inner cylinder and the outer cylinder. Then, the correlation is valid for any Rayleigh and Prandtl number and estimating $Nu_{a_o-g_i}$ is:

$$Nu_{a_o-e_i}=[(Nu_{an\_Cond})^{15}+(Nu_{an\_Conv})^{15}]^{1/15} \tag{27}$$

3-2-3. From Glass Envelope to Environment

As in section 2.3.1.1, this convective heat transfer can also be estimated in accordance with Newton's law of cooling as:

$$Q_{e_o-s\,Conv}=h_{e_o-s}\pi D_{e_o}(T_{e_o}-T_s) \tag{28}$$

$$h_{e_o-s}=\frac{k_{air}}{D_{e_o}}Nu_{D_{e_o}} \tag{29}$$

where, T_s is the temperature of the surroundings, k_{air} is the thermal conductivity of air, h_{e_o-s} is the convective heat transfer coefficient at $(T_{e_o}+T_s)/2$ and $Nu_{D_{e_o}}$ is the Nusselt number evaluated at D_{e_o}.

An approach that utilizes a mixed convection regime (both natural and forced) is employed to estimate the $Nu_{D_{e_o}}$. Primarily, the Nusselt number for natural convection (Nu_N) is calculated as [33]:

$$Nu_N=[(Nu_l)^{10}+(Nu_t)^{10}]^{1/10} \tag{30}$$

where, Nu_l is the Nusselt number for laminar, Nu_t is for turbulent heat transfer from glass envelope, evaluated as [29]:

$$Nu_l=\frac{2\mathcal{F}}{\ln(1+2\mathcal{F}/Nu^T)},$$
$$\text{where } Nu^T=0.772\,C_y Ra_{air}^{1/4} \text{ and } F=1-\frac{0.13}{(Nu^T)^{0.16}} \tag{31}$$

$$Nu_t=C_x Ra_{air}^{1/3} \tag{32}$$

C_x and C_y are constants reliant on Prandtl number (Pr), Ra_{air} is the Rayleigh number based on surrounding air, and Nu^T is the laminar thin layer Nusselt number.

The Nusselt number for heat transfer via forced convection Nu_F is calculated as:

$$Nu_F=\mathcal{U}Re_{air}^{\mathcal{V}} \tag{33}$$

where, Re_{air} is the Reynolds number computed using ambient air properties, $\mathcal{U}$ and $\mathcal{V}$ are chosen from [34].

To encapsulate both convection mechanisms, an equivalent Reynolds number (Re^δ) is determined by applying the identity $Nu_N=Nu_F$, as proposed by [34,35].

$$Re^\delta=[Nu_N/\mathcal{U}]^{1/\mathcal{V}} \tag{34}$$

An overall Reynolds number (Re_{eff}) for the blended flow is then calculated as:

$$Re_{eff}=[(Re^\delta)^2+(Re_{air})^2+2Re_{air}Re^\delta\cos\phi]^{1/2} \tag{35}$$

where, ϕ is the angle between the direction of forced flow and the vertical direction of the natural flow. Now the ($Nu_{D_{g_o}}$) is found by replacing Re_{air} by Re_{eff} in Eq. (34) and the relation turns up as:

$$Nu_{D_{e_o}}=\mathcal{U}Re_{eff}^{\mathcal{V}} \tag{36}$$

3-3. Conductive Heat Transfer

Heat transfer through conduction occurs across a solid surface from high temperature to low temperature and it takes place at three different regions in HCE.

First, through the absorber wall and can be calculated using Fourier's law of conduction [26] as:

$$Q_{a_o-a_i\,Cond}=\frac{2\pi k_{ab}(T_{a_i}-T_{a_o})}{\ln\left(\frac{D_{a_o}}{D_{a_i}}\right)} \tag{37}$$

Here, k_{ab} is the thermal conductivity of absorber calculated at $T_{a_o-a_i}=(T_{a_i}-T_{a_o})/2$.

Second, through the glass envelope which can be evaluated using Eq. (37) with some relevant modifications as:

$$Q_{e_i-e_o\,Cond}=\frac{2\pi k_e(T_{e_i}-T_{e_o})}{\ln\left(\frac{D_{e_o}}{D_{e_i}}\right)} \tag{38}$$

where, k_e is the thermal conductivity of glass envelope.

Third, through the support brackets that are attached to HCE to retain its position. A part of heat is conducted ($Q_{Brac-Cond}$) to these and is lost to the ambient through convection ($Q_{Brac-Conv}$) and radiation ($Q_{Brac-Rad}$). To estimate this loss, the following correlations are used:

$$Q_{Brac-Conv}=(\sqrt{h_{Brac-s}P_{Brac}k_{Brac}A_{Brac}}(T_{Brac}-T_s)\tan mL)/L \tag{39}$$

$$Q_{Brac-Rad}=\sigma\varepsilon_{Brac}P_{Brac}(T_{Brac}^4-T_{sky}^4) \tag{40}$$

$$Q_{Brac-Cond}=Q_{Brac-Rad}+Q_{Brac-Conv} \tag{41}$$

where, $m=\sqrt{h_{Brac-s}P_{Brac}/k_{Brac}A_{Brac}}$, L is the length, A_{Brac} is the area of cross-section, and P_{Brac} is the perimeter of the support bracket. In addition, h_{Brac-s} is the convective heat transfer coefficient between brackets and ambient, and is calculated using the method discussed in Section 2.3.1.3. Also, k_{Brac} is the thermal conductivity of support bracket and is evaluated using the following correlation derived for plain carbon steel [36].

$$k_{Brac}=-0.0419T_{Brac}+73.235 \tag{42}$$

4. PTSC Efficiency

Now, the efficiency of PTSC can be obtained as:

$$Q_{ug}=\frac{dm_f}{dt}C_{pf}(T_{out}-T_{in}) \tag{43}$$

$$\eta=\frac{Q_{ug}}{(DNI)A_{cl}} \tag{44}$$

where, dm_f/dt, C_{pf} are, respectively, mass flow rate and specific heat capacity of HTF, and Q_{ug} is the total heat gain by HTF.

As stated before, heat transfer terms are evaluated radially. After this, by using the steady-state energy balance for receiver (divided into "N" segments), T_{out} for k^{th} segment of HCE can be estimated by

$$T_{out,\,k}=T_{in,\,k}+\frac{\left(\frac{Q_{Ab}-Q_{loss}}{\Delta l_{hce}}-Q_{Brac-Cond}\right)}{\frac{dm_f}{dt}C_{pf}} \tag{45}$$

Here, $T_{in,k}$ is the temperature of HTF entering the HCE (at k=1). $T_{out,N}$ at k=N will be temperature of HTF leaving the HCE, i.e., exit temperature (T_{out}). Q_{Ab} is the solar energy absorbed by HCE, and Q_{loss} is the heat energy lost to the environment.

MODEL VALIDATION

Obtained simulation results were compared with experimental results from three different PTSC setups to validate the proposed model:

- **SEGS LS-2** [22] A module of Luz system second generation (LS-2) collector which is generally used in solar electric generating system (SEGS) plants was tested at Sandia National Laboratory (SNL). Tests were conducted for two different SSACs (cermet and black chrome) with different annulus conditions (vacuum intact and lost).
- **IST PTSC** [23] A single mirror module of industrial solar technology (IST) collector was tested for thermal performance at SNL. Two different glass envelopes, borosilicate Pyrex glass and a solgel anti-reflective (AR) coated Pyrex glass, were used in testing. Also, two different SSACs (black chrome and black nickel) were involved.
- **HTF test bench** [24,37] This is located at Plataforma Solar de Almería (PSA), Spain, and is meant for evaluating PTSC components under real solar energy operating conditions. The facility is well instrumented and is ideal for testing collectors up to 75 m long, different HCEs, tracking systems, and so on.

Table 1 depicts the contrasting geometric specifications of each of the setups discussed above. A MATLAB script was created to incorporate the geometric values and physical properties for each setup. The model was then simulated in MATLAB and solved using direct solvers available in it.

To run the model and evaluate the thermal performance of PTSC, it is a prerequisite that HTF type and its physical properties are known. Here, in all the setups, Syltherm 800 was used as HTF.

For SEGS LS-2 collector, the model was run for all four cases

Table 1. Geometrical parameters used for model validation

	SEGS LS-2 [22]	IST PTSC [23]	HTF test bench [24,37]
Collector length, l_{cl}	7.8 m	6.1 m	75 m
Collector width, w_{cl}	5 m	2.3 m	5.76 m
Inner diameter of absorber, D_{a_i}	0.066 m	0.051 m	0.066 m
Outer diameter of absorber, D_{a_o}	0.070 m	0.0476 m	0.070 m
Inner diameter of glass envelope, D_{e_i}	0.109 m	0.069 m	0.120 m
Outer diameter of glass envelope, D_{e_o}	0.115 m	0.075 m	0.125 m
Length of HCE, l_{hce}	8 m	6.1 m	4.06*18 m
Collector aperture area, A_{cl}	39.2 m^2	13.2 m^2	409.908 m^2

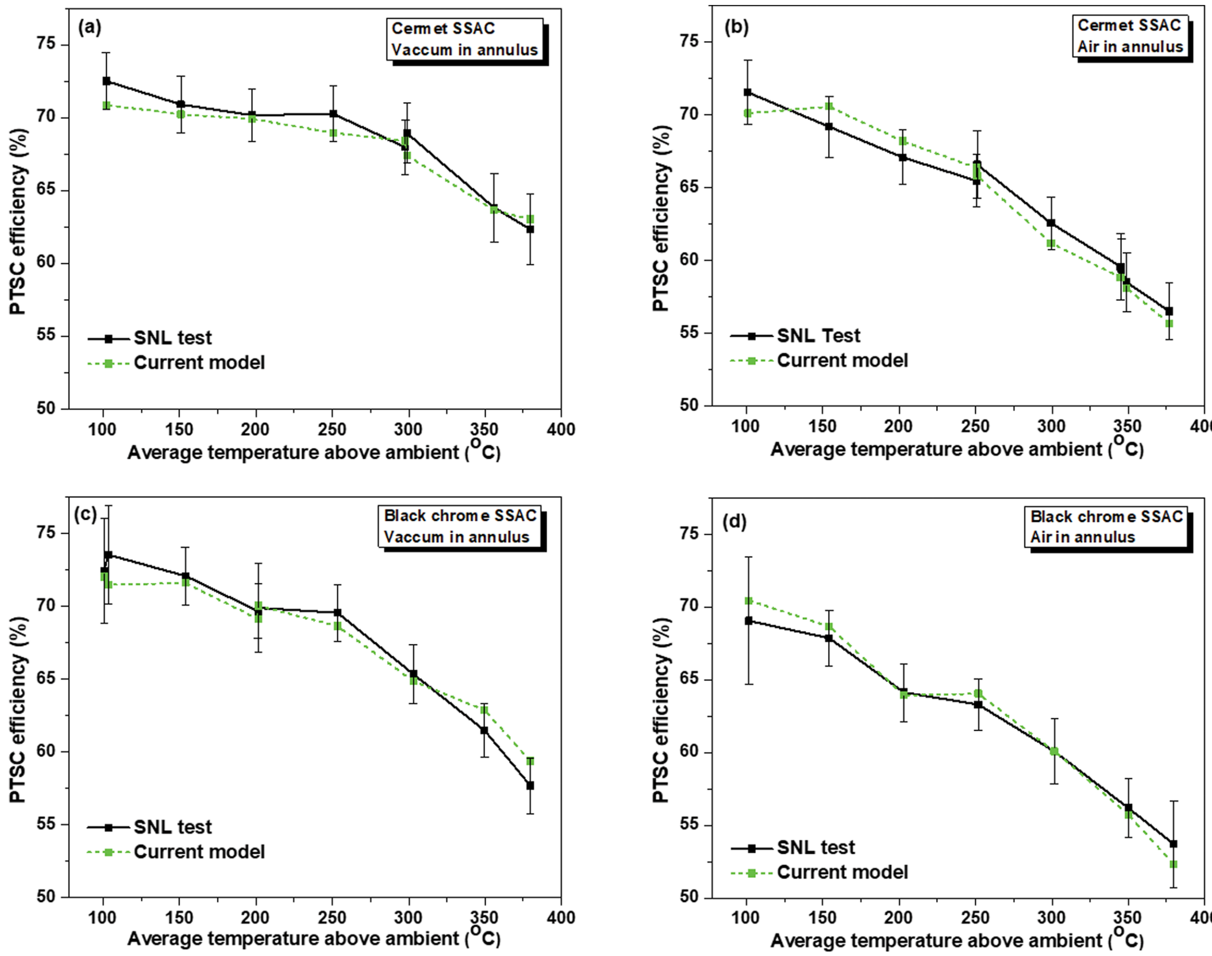

Fig. 2. Comparison between efficiency estimations by proposed model and measurements of SNL tests versus HTF inlet temperature, for different cases: (a) and (b) cermet coating, (c) and (d) black chrome coating.

viable with mentioned SSAC types and conditions of vacuum. Fig. 2 shows a comparison between the results obtained through proposed model and the experimental results by SNL. Each point on the solid line represents the thermal efficiency of PTSC obtained by SNL at several input variables such as ambient temperature, HTF flow rate, solar irradiation, inlet HTF temperature, and wind speed. Many of these inputs are environmental factors that cannot be controlled. Also, as shown in Table A1-A4 (see appendix), the experimental results for SEGS LS-2 are obtained at random conditions, so they may not be expected to follow a smooth path. The model was simulated for the reported conditions and proficiently follows the experimental outputs, culminating in uneven shapes shown in Fig. 2.

All values were found to be within the error bars for the experimental uncertainty. However, small deviations in the estimations (over or under) can be witnessed, which could be due to:

- As can be noticed in Section 2, different correlations have been utilized to estimate various heat transfers. Each of them is derived with some approximations and assumptions, which can lead to inconsistency. For example, depending upon the annulus condition, two different sets of correlations have been utilized to estimate the convective heat transfer in annulus region (see Section 2.3.2.2). Evidently, model estimations are seen to be distinct at temperatures >350 °C. It slightly overestimates with vacuum in annulus and marginally underestimates with air in annulus.
- Propagation of error can be caused by the uncertainties in the correlations used for physical properties of absorber materials, SSACs, HTF, and surrounding air. For instance, correlations used to calculate emittance SSACs (cermet and black chrome) are taken from [20] and are only derived through two data points. Thus estimations for radiative heat transfer will possibly have errors.
- Another potential cause of model divergence involves the assumptions made while drafting it. Such as temperature gradients are considered in radial direction only, constant dimensions (diameter, length, etc.) during operation, fluids are incompressible, flux distribution is uniform throughout the HCE, and others.

The model predictions were found to be faithful to all the necessary assumptions. A better judgment about the accuracy of estimations made by the model can be made by looking at the root mean square error (RMSE) for all four cases as follows: vacuumed annulus, cermet SSAC=0.990; vacuumed annulus, black chrome SSAC=1.045; air in annulus, cermet SSAC=1.010; and air in annulus, black chrome SSAC=0.874. All the RMSE values are less than

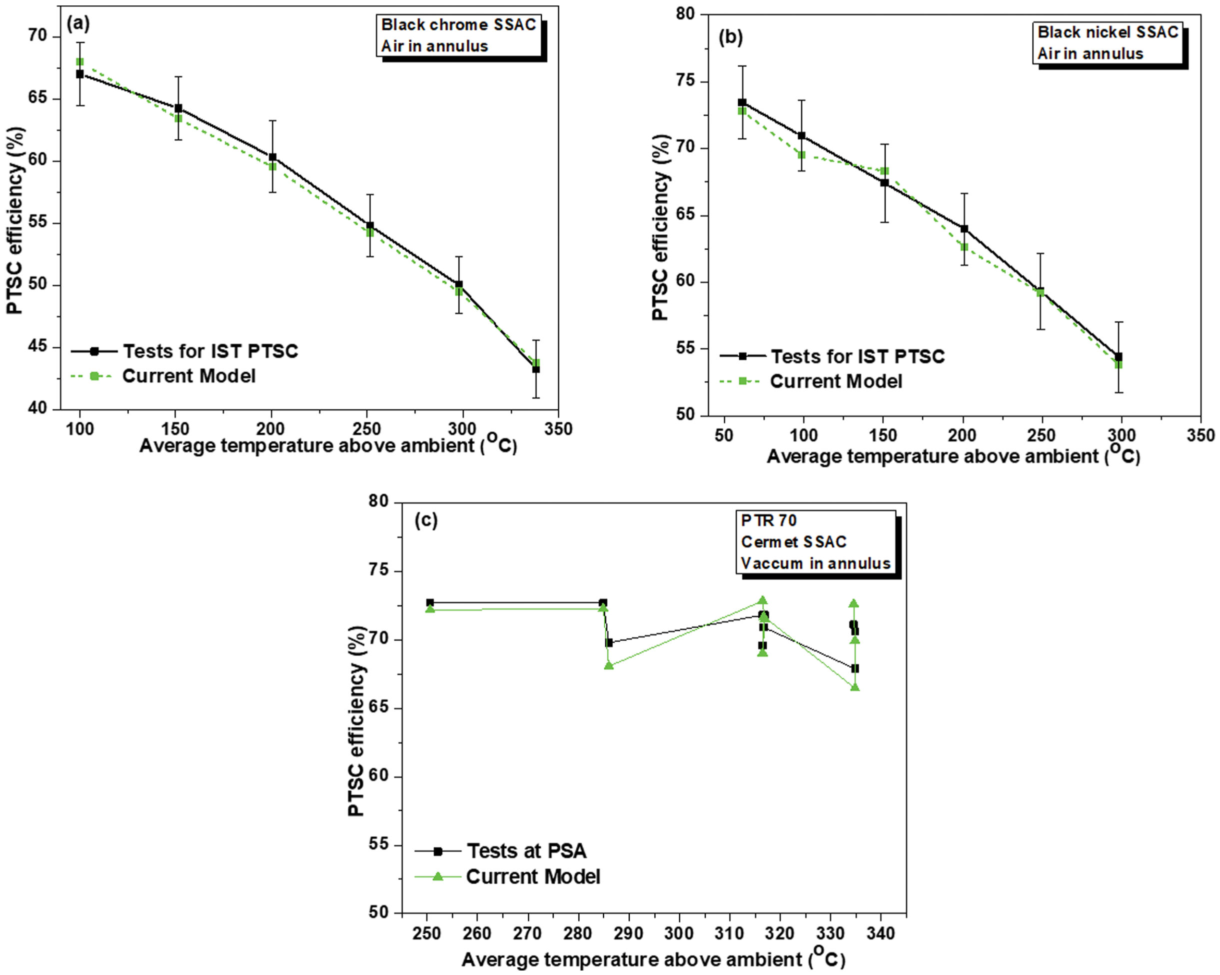

Fig. 3. Comparison between efficiency estimations by proposed model and experimental measurements versus HTF inlet temperature, for (a) IST PTSC, black chrome SSAC, (b) IST PTSC, black nickel SSAC, and (c) HTF test bench, Cermet SSAC.

or close to unity, suggesting that the current model provides worthy estimation for every case, hence confirming the good accuracy of the model.

Further, the model is utilized to estimate the efficiency for IST PTSC in two cases:

- Black chrome SSAC, simple Pyrex glass (without AR coating).
- Black nickel SSAC, Solel Glass with AR coating.

Efficiency predictions made by the current model for the mentioned cases are presented in Figs. 3(a) and 3(b), respectively. It is evident that the current model is making effective and accurate estimations for both cases. Estimations are found to be well within the experimental uncertainty bars, and again they follow the experimental results in Table A5-A6 (see appendix) for IST PTSC. The model has proven to be quite precise, with an RMSE value of 0.722 and 0.944 in respective cases. Although, slight errors in the model estimations are certainly due to the reasons mentioned previously.

The above discussed setups are single PTSC modules, while for practical applications an array of such modules is required. So, additionally, to check the proficiency of the current model, it is employed to make the estimations for the HTF test bench at PSA labs, which is geometrically much bigger. It operates with PTR®70 receiver, which has a cermet coated 316L stainless steel absorber with vacuumed annulus along the Pyrex glass tube [37]. The estimates for the same are obtained by the current model and manifested in Fig. 3(c). It shows that the current model upholds its accuracy, and the deviations in estimated values from the experimental ones are minute with an acceptable RMSE value (1.015). The experimental conditions and results reported for the HTF test bench are shown in Table A7 (see appendix). The proposed model was simulated for the same conditions and, as seen, the obtained results closely follow the trend of experimental results. Minor differences in model and experimental values are due to the prior discussed reasons.

It is interesting that in Fig. 3(c), two places show three or more data at the same temperature, but the value of efficiency is different. They have different efficiencies because few other input parameters are different, which can be recognized through Table A7 (see appendix). The major cause of the difference in efficiency at almost similar inlet HTF temperatures is the change in the angle of incidence (θ). For instance, it can be ascertained that data points at same temperature 334.8 °C (in Table A7) have similar input flow rates, ambient temperature (T_{amb}), and DNI but still have different output efficiencies. This is because one of them has a high value of θ as input. As per Eqs. (1) to (4), a higher value of θ means that the value of factors like incidence angle modifier and end loss tends to get lower, which is normally unity or close to it. Thus, according to Eqs. (6) and (9) optical efficiency degrades and solar energy absorbed by the absorber is reduced (Eq. (8)), leading to lower thermal efficiency (Eq. (44)).

Overall, after testing the current model for three different setups involving the contrasting geometries and operating conditions, it can be said that the current model has reliable performance. The tested setups involved three different SSACs (cermet, black chrome, black nickel), two different glass envelopes (Pyrex and Solel), and two different annulus conditions (vacuum and air), yet the model performance was unaffected. Thus, it can be deduced that the current model is reliable enough to be utilized for analysis and optimization purposes for PTSC.

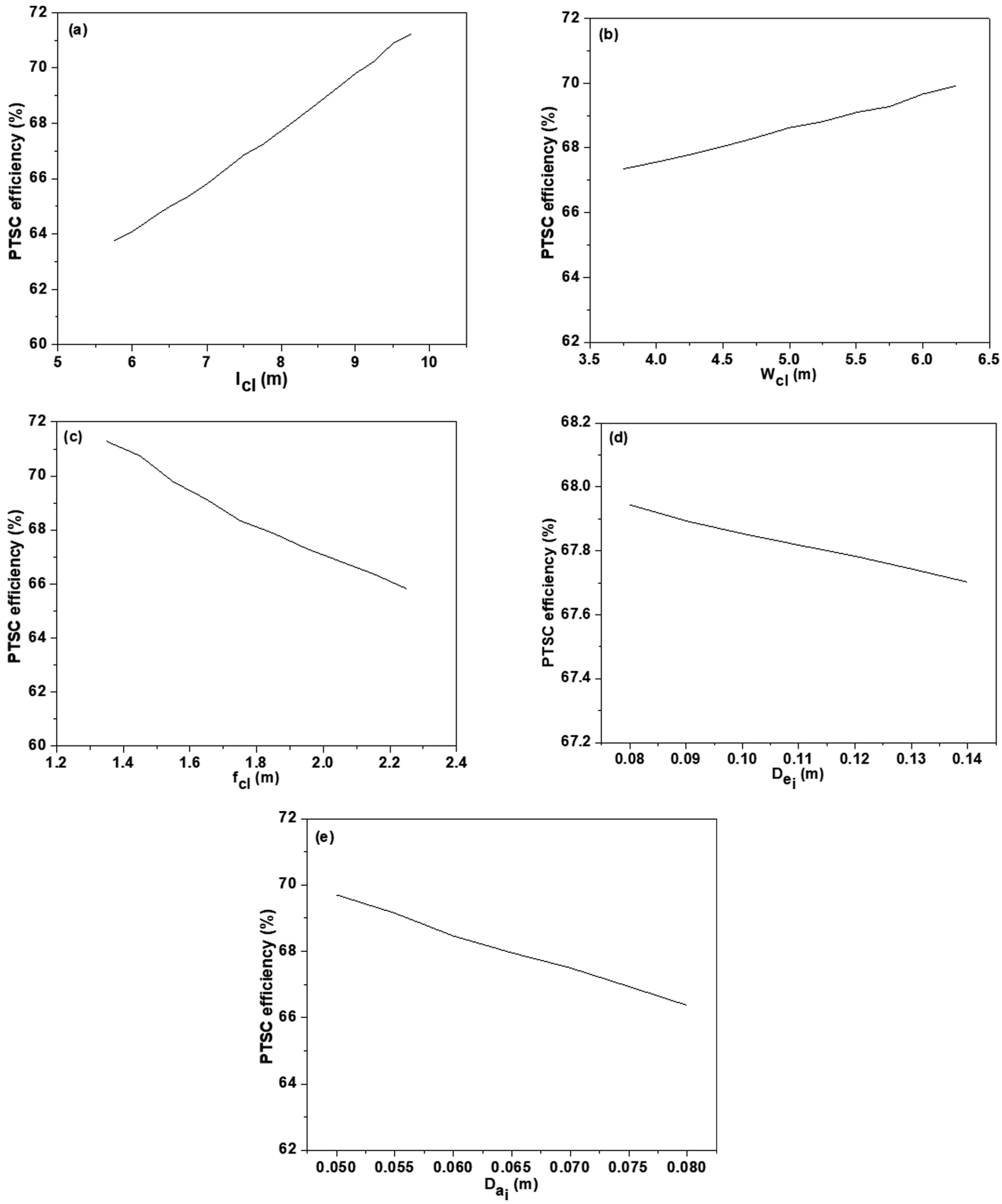

Fig. 4. Variation in efficiency of PTSC versus (a) collector length, (b) collector width, (c) focal length of collector, (d) inner diameter of glass envelope, and (e) inner diameter of the absorber.

RESULTS AND DISCUSSION

1. Sensitivity Analysis

First, the effect of variation in geometrical parameters of PTSC on its efficiency is analyzed here. Geometrical parameters (l_{cl}, w_{cl}, f_{cl}, D_{e_i}, D_{a_i}) were varied one by one to study their impact on the PTSC efficiency. One geometrical term was varied at a time while others were kept fixed with base values mentioned in Table 1 for SEGS LS-2. Physical parameters were also kept constant, as the motive was to study the impact of geometric variations only. Different physical parameters which are required as input along with their used value here are: inlet HTF temperature=150 °C, wind speed=3 m/s, T_s=27 °C, HTF flow rate=50 L/Min, DNI=900 W/m^2.

The variation of PTSC efficiency with the collector length (l_{cl}) is shown in Fig. 4(a) and with collector width (w_{cl}) in Fig. 4(b). As the l_{cl} or w_{cl} increases, considering Eqs. (7) to (9), the overall collector area (A_{cl}) also increases which increases the DNI received and hence improves the optical efficiency (η_{O-ab}). This means high solar absorption and higher HTF temperature at outlet, thus increasing PTSC efficiency, as noticeable in Fig. 4(a). As l_{cl} is increased from 5.75 m to 9.75 m, efficiency is increased by ~7.5%, while an increase in w_{cl} from 3.75 m to 6.25 m leads to ~2.5% rise in efficiency. So, it can be concluded that effect of increase in l_{cl} is more prominent than increase in w_{cl}.

Fig. 4(c) depicts that increase in focal length (f_{cl}) of the collector reduces the PTSC efficiency, a decline of ~5% can be seen as f_{cl} is increased from 1.35 m to 2.25 m. According to Eqs. (4) and (6), increase in f_{cl} enhances the effect of end loss and diminishes the optical efficiency, which means less solar absorption. Besides, as discussed in section 2.3.3.3, larger focal length means higher heat loss through support brackets. It is to be noted that due to optical constraints, too much decrease in f_{cl} is also not advisable, as appropriate reflection of solar beam is necessary for stable operation.

Effect of varying the inner diameter of glass envelope (D_{e_i}) over the PTSC efficiency is shown in Fig. 4(d). Increase in D_{e_i} causes enlarged annulus gap, thus reducing the heat transfer from absorber to glass envelope but surface area of envelope is increased, leading to more heat loss to surroundings. Also, reducing D_{e_i} can lower the surface area and loss to surroundings, but small annulus gap can damage HCE, as it tends to bow when heated. It is realized that the effect of change in D_{e_i} is minor, as only an decrease of ~0.24% is seen as D_{e_i} is increased from 0.08 m to 0.14 m.

A change in PTSC efficiency with inner diameter of absorber (D_{a_i}) is demonstrated in Fig. 4(e). Increase in D_{a_i} causes the follow-

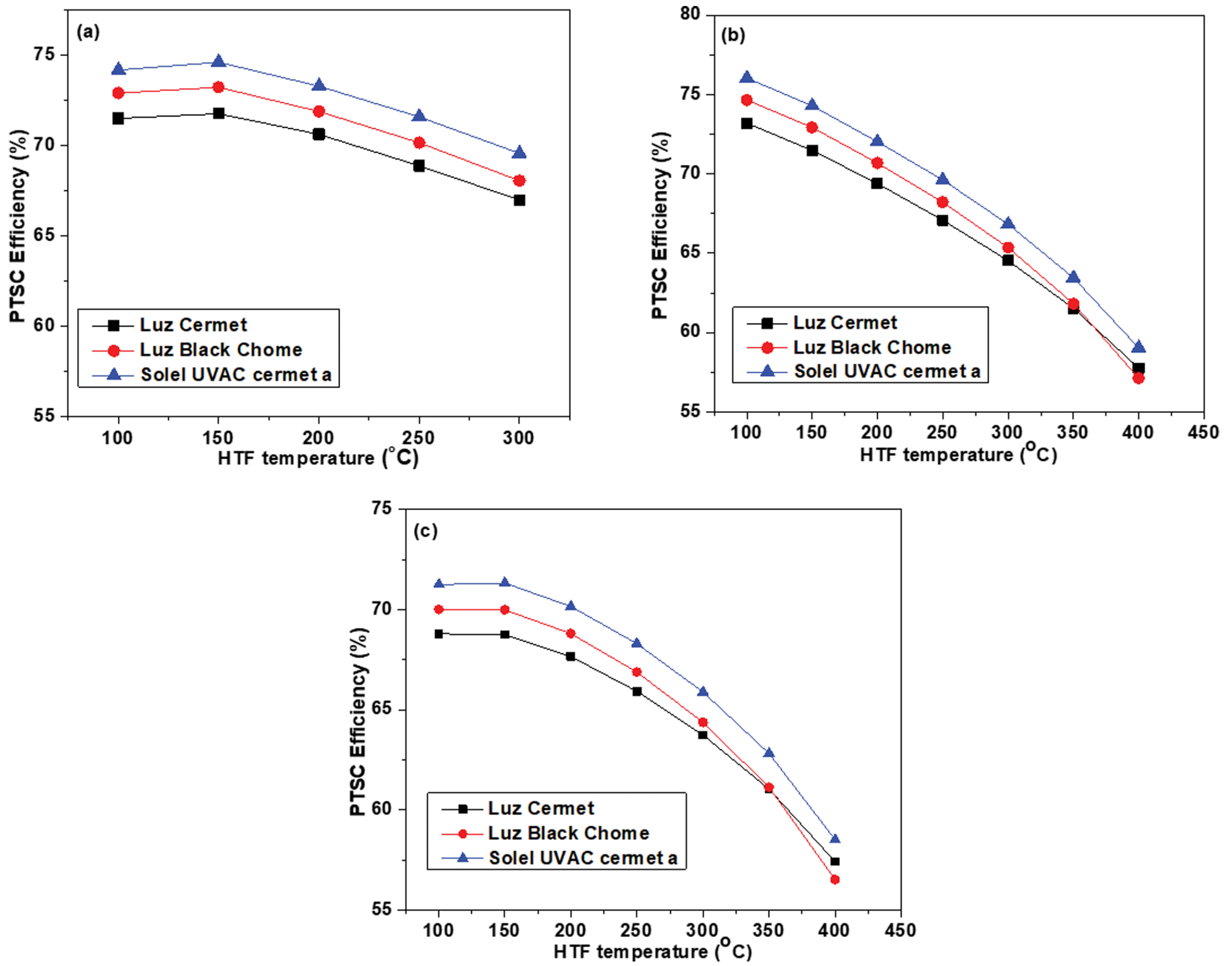

Fig. 5. Variation in efficiency of PTSC with different SSACs along (a) Xceltherm 600, 321H; (b) Therminol VP1, 321H; and (c) Syltherm 800, 321H.

ing effects:

- Drop in convective heat transfer coefficient (h_f) as per Eq. (18).
- Boost in heat transfer from absorber surface to glass envelope, as annulus gap will reduce.
- According to Eq. (19), increase in Nusselt number ($Nu_{D_{a_i}}$) for convective heat transfer in absorber.

Overall effect is seen as decrease in PTSC efficiency with increase in D_{a_i} which is due to the combination of the above effects. An decrease of ~3% is observed as D_{a_i} increased from 0.05 m to 0.08 m.

As discussed in section 2.1, PTSC comprises several design components that perform specific tasks to make it functionally operated. Components such as SSAC, HTF, and absorber material influence the PTSC efficiency. Various types are available for each of them, with every type having distinct properties. Thus, pertaining to the physical properties, a combination of these design components will affect the PTSC efficiency. The effects of three SSACs (Luz cermet, Luz black chrome, and Solel UVAC cermet a), three HTFs (Syltherm 800, Therminol VP1, and Xceltherm 600), and three absorber materials (stainless steel 321H, 304L, and 316L) are examined here. The mentioned types for each of the components considered here are the ones that are widely tested in different studies, but their sensitivity analysis with this perception has been overlooked earlier.

The effect of switching the different SSACs at different HTFs along with 321H stainless steel absorber over the PTSC efficiency is shown in Fig. 5. Each SSAC has distinct optical properties in terms of absorptance and emittance values. For good solar energy absorption by absorber tube, an SSAC should have high absorptance and low emittance. It can be seen that the type of SSAC has strong influence on the performance of PTSC: better optical properties cause higher efficiency. Solel UVAC cermet has better absorptance and emittance values and shows clear improvement in efficiency compared to Luz coatings. Same trend can be witnessed at each HTF; only the value of efficiency at a particular temperature is changed depending upon the properties of HTF. For example, at 100 °C, PTSC comprising Solel coating with Syltherm 800 has an efficiency of 71.25%, while 74.18% with Xceltherm 600 and 76.04% with Therminol VP1. Although luz chrome has better absorptance than luz cermet, but due to its higher emittance above 350 °C, efficiency lags are noticed and Luz cermet looks a slightly better option at higher temperature.

The influence of changing the HTFs at different SSACs along

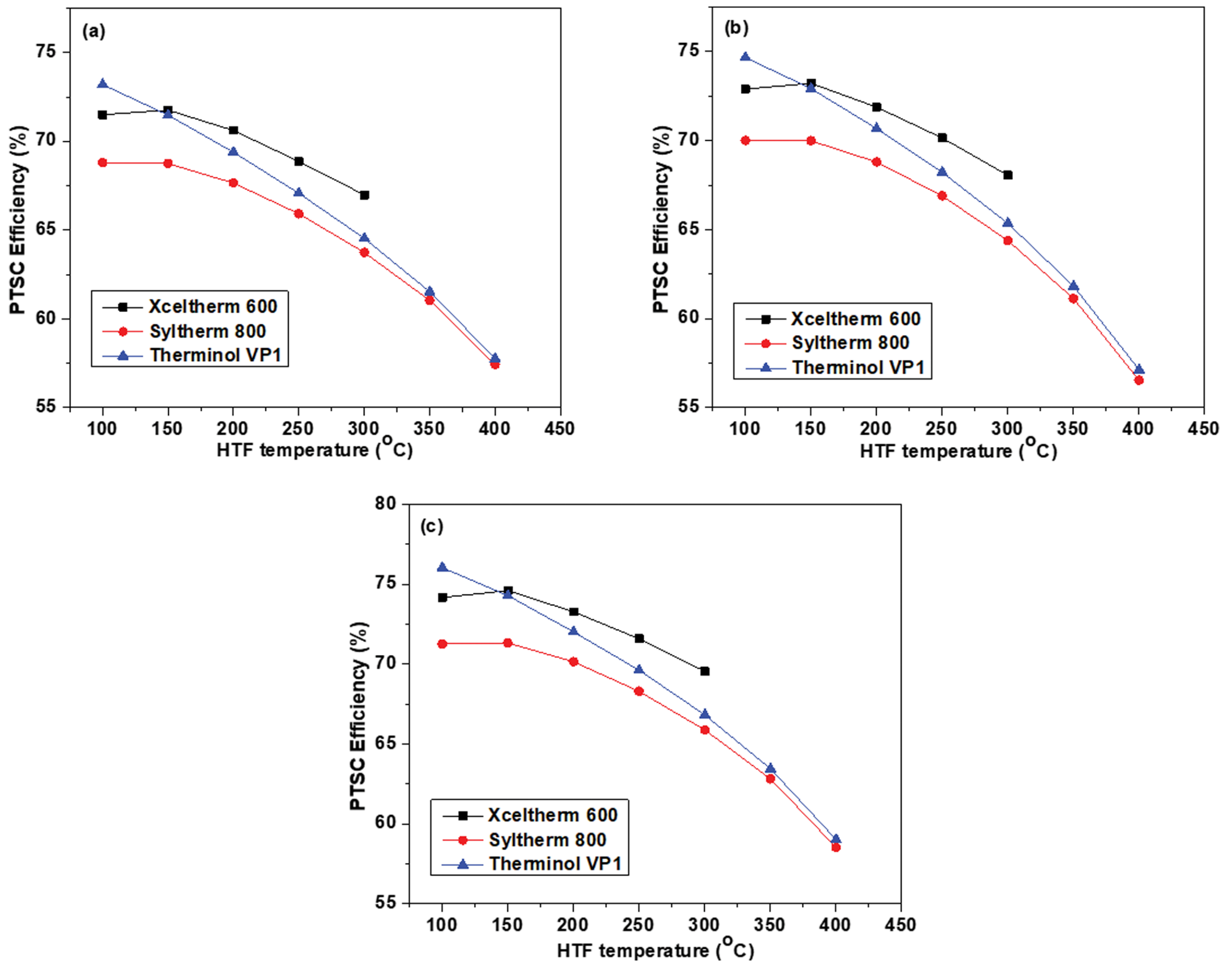

Fig. 6. Variation in efficiency of PTSC with different HTFs along (a) Luz cermet, 321H; (b) Luz black chrome, 321H; and (c) Solel UVAC cermet a, 321H.

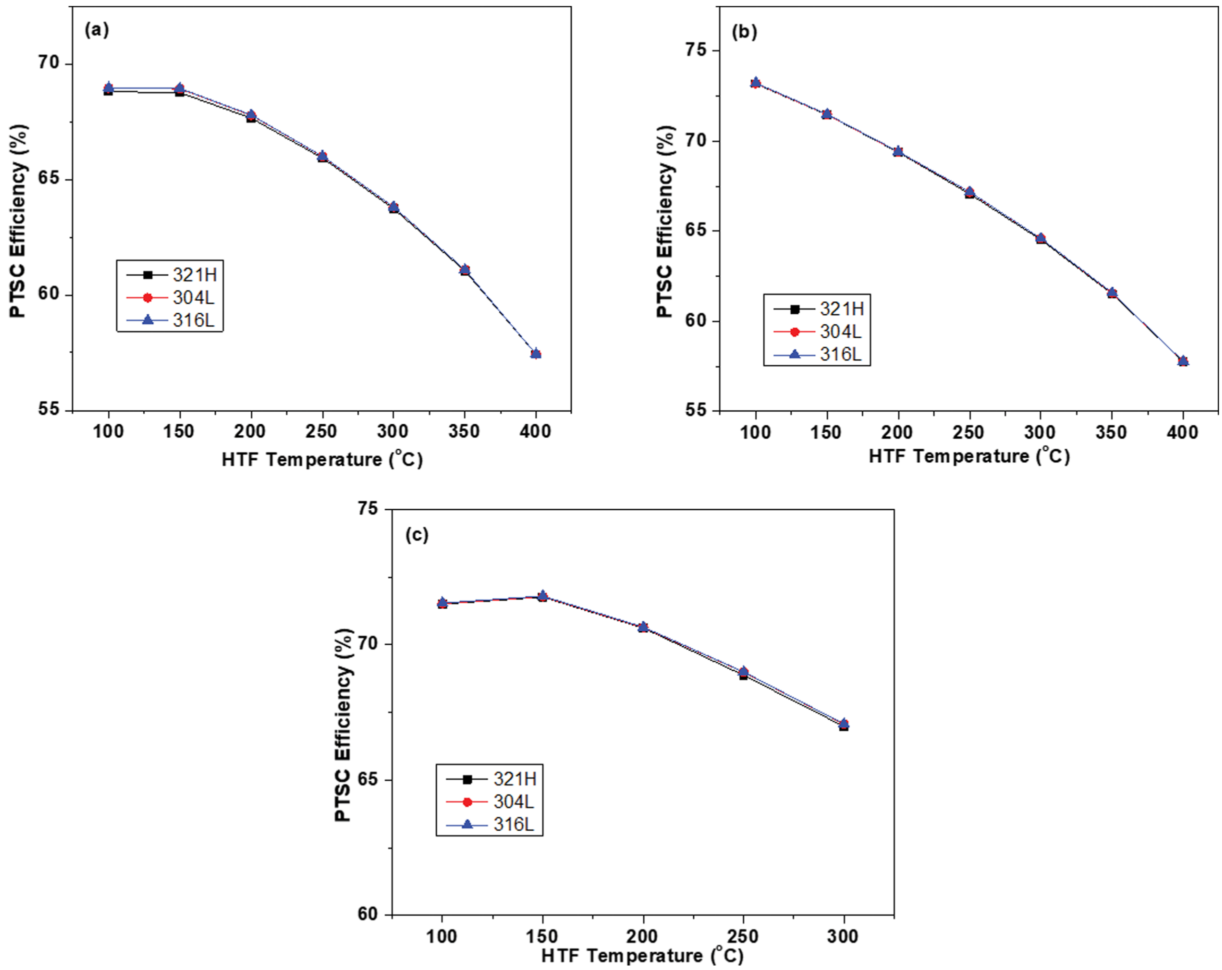

Fig. 7. Variation in efficiency of PTSC versus HTF temperature at different absorber materials with (a) Syltherm 800, Luz cermet; (b) Therminol VP1, Luz cermet; and (c) Xceltherm 600, Luz cermet.

with 321H stainless steel absorber on the thermal efficiency of PTSC is shown in Fig. 6. Physical properties of HTF, namely density (ρ_f), specific heat (C_{pf}), thermal conductivity (k_f), and viscosity (μ_f), vary with temperature and, depending upon that, the PTSC efficiency fluctuates. It can be realized from Fig. 6 that none of the HTFs have clear supremacy over the others. With the increase in temperature, the best fit HTF is swapping, from 100 °C to 125 °C, Therminol VP1 looks best; from 200 °C to 225 °C, Xceltherm 600 looks best. Above 350 °C, Xceltherm 600 does not work as it starts to degrade at 310 °C, but Therminol VP1 and Syltherm 800 both look equally promising; the same trend is followed with different SSACs. Albeit, with the change in SSAC, the curves for HTFs are shifted depending upon the optical properties of it. For instance, at 100 °C, PTSC using Syltherm 800 as HTF with Luz cermet has an efficiency of 68.79%, while it is 70.00% with Luz black chrome and 71.25% with Solel coating.

Fig. 7 shows the variations in efficiency of a PTSC while replacing different absorber materials at different HTFs along with Luz cermet SSAC. Here, three different varieties of stainless steel are analyzed, which are different by composition and thermal conductivity. It can be followed that PTSC efficiency is faintly affected by change in absorber material. For example, at 150 °C, PTSC utilizing Syltherm 800 as HTF and Luz cermet as SSAC, the efficiency is 68.92% with 304L, 68.94% with 316L, and 68.75% with 321H. A change in HTF is just shifting the curve according to its properties, but the effect of change in absorber material is vague. Although, while choosing the absorber material, its corrosive properties, strength, ease of installation and coating, need to be further analyzed.

To get a clearer picture about the effect of the combination of design components, PTSC efficiency is noted for various combinations at 150 °C, as shown in Table 2.

For obtaining the highest efficiency, combination 7 and 9 are the best options, both are providing almost similar efficiency of 74.61% and 74.28%. Similar analysis was done for the above mentioned combinations at 100 °C and it was found that combination 9 gives highest efficiency of 76.04% and next best is combination 6 with efficiency of 74.48% ~ combination 7 with efficiency of 74.38%. Combinations 7 and 9 are competitive options at 150 °C, while at 100 °C combination 9 is clearly better than 7. Both the combinations have same SSAC and absorber material, but HTFs are different. This means that variation in the physical properties of HTF with temperature is affecting the choice of best combination here. To attain better understanding of this, their thermal properties are

Table 2. Various combinations of design components

Combination	HTF	SSAC	Absorber material	PTSC efficiency (%)
Comb. 1	Xceltherm 600	Luz Cermet	321H	71.76
Comb. 2	Syltherm 800	Luz Cermet	321H	68.75
Comb. 3	Therminol VP1	Luz Cermet	321H	71.47
Comb. 4	Xceltherm 600	Luz black chrome	321H	73.22
Comb. 5	Syltherm 800	Luz black chrome	321H	69.98
Comb. 6	Therminol VP1	Luz black chrome	321H	72.93
Comb. 7	Xceltherm 600	Solel UVAC cermet a	321H	74.61
Comb. 8	Syltherm 800	Solel UVAC cermet a	321H	71.33
Comb. 9	Therminol VP1	Solel UVAC cermet a	321H	74.28

Table 3. Comparison of thermal properties between Xceltherm 600 and Therminol VP1

Xceltherm 600 v/s Therminol VP1	At 100 °C	At 150 °C
Thermal conductivity (k_f) (W/m k)	0.1297-0.1277	0.1257-0.1212
Specific heat capacity (C_{pf}) (J/kg·K)	2,266>1,775	2,436>1,913
Density (ρ_f) (kg/m^3)	804<999	773.6<957
Dynamic viscosity (μ_f) (mPa·s)	2.432>0.985	1.085>0.585

compared in Table 3.

All these properties majorly impact convective heat transfer to HTF ($Q_{a_i-f\,Conv}$); better $Q_{a_i-f\,Conv}$ reflects higher heat gain by HTF, thus higher thermal efficiency (η). Here, the value of k_f is nearly equal for both the HTFs and at both the temperatures, so it cannot contribute much to the variation in η.

C_{pf} and μ_f can alter the Prandtl number ($Pr_f=\mu_f C_{pf}/k_f$); increase in their value means increase in Pr_f which as per Eqs. (17), (18), and (19) leads to higher value of $Nu_{D_{a_i}}$, thus increased h_f and $Q_{a_i-f\,Conv}$ leading to better efficiency. High C_{pf} also suggests better heat gain $Q_{ug}=\frac{dm_f}{dt}C_{pf}(T_{out}-T_{in})$, thus elevation in η (as per Eq. (44)). In the current case, at both the temperatures Xceltherm 600 has higher value of C_{pf} and μ_f, which means better efficiency.

Another effect can be endured by $Re_{D_{a_i}}=\rho_f v D_{a_i}/\mu_f$ due to ρ_f and μ_f, having an opposing impact on it. For the situation under observation, at both the temperatures, Xceltherm 600 has lower value of ρ_f and higher value of μ_f in comparison to Therminol VP1. In this case, it results in decrease of $Re_{D_{a_i}}$ for Xceltherm 600. According to Eqs. (19) and (20) this means rise in $Nu_{D_{a_i}}$ and fr leading to rise in efficiency. Deviation in ρ_f also impacts $m_f=\rho_f v\pi/4(D_{a_i}^2)$, which in turn alters the Q_{ug}. For the case discussed here, lower value of ρ_f for Xceltherm 600 means reduced m_f and Q_{ug} resulting in lower efficiency.

Overall, for Xceltherm 600, k_f has close values at both the temperatures and does not have much impact on efficiency (no effect), C_{pf} and μ_f have higher values which promise higher efficiency (positive effects), ρ_f has lower values and contributes to an increase as well decrease in efficiency (positive and negative effect).

From the above discussion it seems like combination 7 (Xceltherm 600+Solel coating+321H) should be more efficient than combination 9 (Therminol VP1+Solel coating+321H) at both temperatures. Although, at 150 °C: Xceltherm 600 is just slightly more efficient than Therminol VP1, which means that positive and negative effects of its thermal parameters are almost at par with a minor edge of positive effect. At 100 °C, Xceltherm 600 is clearly less efficient than Therminol VP1, which suggests that the negative effect of its thermal parameters is dominating the positive effect.

It can be inferred that better appearing properties of the design component cannot guarantee better performance, as there are many interacting factors. Also, a particular combination can perform better at a certain temperature than the others. Moreover, the above analysis included only three HTFs, three SSACs, and a single absorber material, resulting in only nine (3*3*1) distinct combinations studied at two temperatures. As type of design components (HTF, SSAC, and absorber material) increases, more discrepan-

Table 4. Optical properties of different SSACs [22,23]

SSAC	Absorptance (α)	Correlation for emittance (ε)
Luz Black Chrome	0.94	$\varepsilon_{a_o}=0.0005333(T+273.15)-0.0856$
Luz Cermet	0.92	$\varepsilon_{a_o}=0.000327(T+273.15)-0.065971$
Solel UVAC Cermet avg	0.955	$\varepsilon_{a_o}=(1.907*10^{-7})T^2+(1.208*10^{-4})T+6.282*10^{-2}$
Solel UVAC Cermet a	0.96	$\varepsilon_{a_o}=(2.249*10^{-7})T^2+(1.039*10^{-4})T+5.599*10^{-2}$
Solel UVAC Cermet b	0.95	$\varepsilon_{a_o}=(1.565*10^{-7})T^2+(1.376*10^{-4})T+6.966*10^{-2}$
Black nickel	0.97	$\varepsilon_{a_o}=0.0008(T+273.15)-0.06$

cies can be found and the problem becomes more complex. Thus, this calls for an optimal analysis to suggest a prime combination of design components depending upon the application of PTSC and operating temperature.

2. Combinatorial Optimization

It was observed in the previous section that various interrelated factors govern the operation of PTSC. Choosing a design component just by regarding its properties cannot guarantee improved efficiency. Besides, a specific combination of components can deliver better efficiency at certain temperatures than the others. Thus, there is a need to search for an optimal combination of components depending upon the application and operating temperature of the

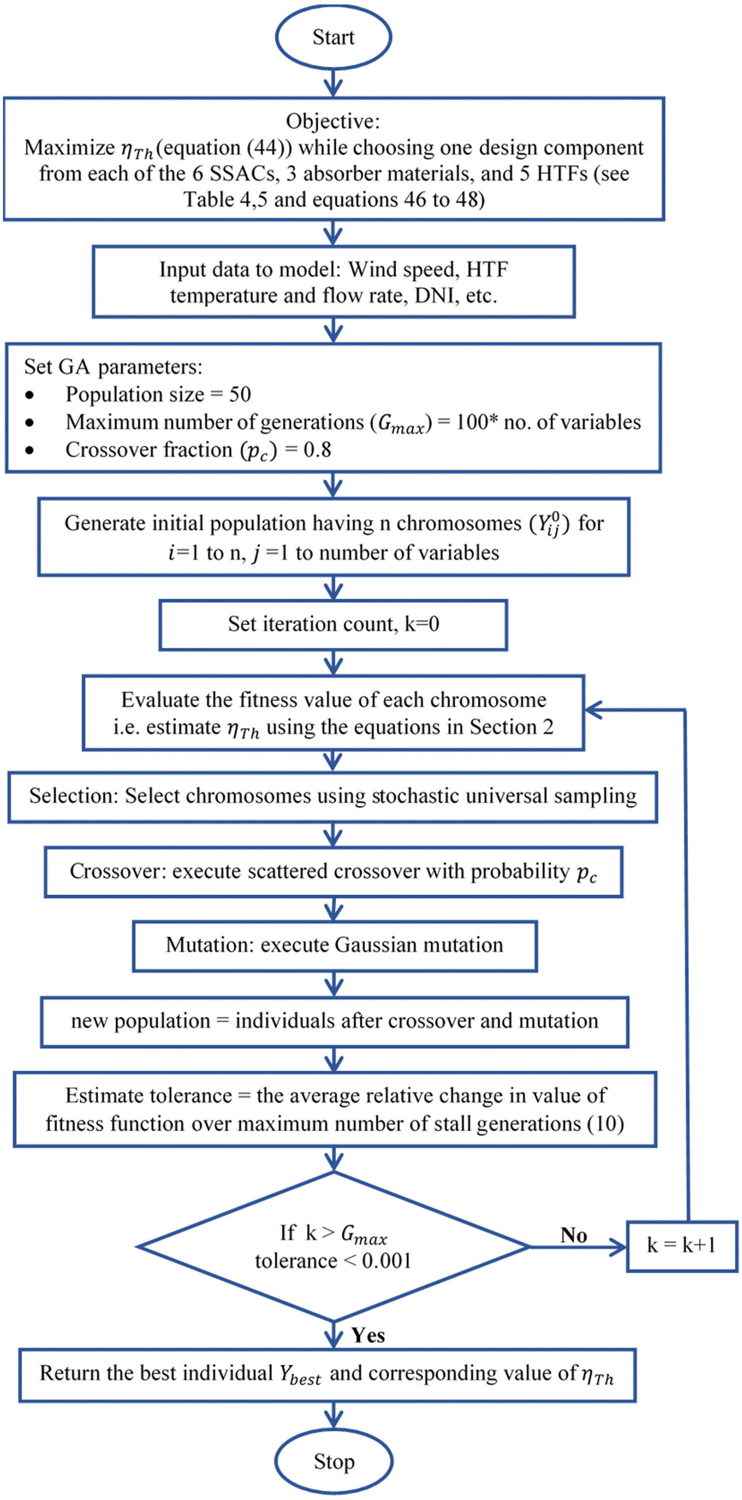

Fig. 8. Optimization procedure to determine the best combination of design components using GA.

PTSC system.

The problem of finding an optimal object from a finite set of objects comes under combinatorial optimization. In many such problems, exhaustive search is found to be untractable and MILP/meta-heuristic approaches are often essential. Here, to highlight the need for combinatorial optimization, a search for an optimal combination of design components was carried out using the genetic algorithm (GA) in MATLAB environment. In the current problem, the objective function does not depend directly on the decision variables considered here. GA can be used for optimization of such cases and hence employed [38]. A detailed optimization procedure followed to determine the best combination of design components using GA is shown in Fig. 8.

The best combination was searched among six SSACs, three absorber materials, and five HTFs, leading to a reasonably big set of 90 combinations. Setup considered for analysis is SEGS LS-2 collector with geometric parameters mentioned in Table 1. To observe the improvement in efficiency, a base case comprising cermet coating with vacuum intact was reviewed with such physical parameters as inlet HTF temperature=150 °C/300 °C, wind speed=3 m/s, T_s=27 °C, HTF flow rate=50 L/Min, DNI=900 W/m^2, and efficiency=68.90%/63.78% at these. Various design components examined in this study along with their physical properties and required empirical correlations, are indicated hereafter.

SSACs have reasonable impact on the performance of PTSC, and it is crucial to employ an adequate SSAC with stable optical conditions for appropriate operation. Table 4 shows different SSACs along with their optical properties. It is to be noted that for SSAC, absorptance is a constant value, while emittance is a function of temperature.

As already indicated, change in absorber material does not have a significant effect on the PTSC efficiency. Still, as this study is confined to the usage of PTSC in industries, it cannot be neglected here, as even a small improvement can lead to reasonable benefits. Commonly used absorber material is stainless steel; its types used for manufacturing HCEs are 304L, 316L, and 321H. Among the physical properties, it is the thermal conductivity (k_{ab}) of the absorber that affects the thermal efficiency of the PTSC. k_{ab} is temperature dependent and empirical correlations required for it are [20,39]:

Table 5. Empirical relations for different properties of HTF

Heat transfer fluid (HTF)	Empirical relations
Syltherm 800 [40]	$\rho_f=953.2-0.9166\times T+4.21\times10^{-4}\times T^2-1.671\times10^{-6}\times T^3$ $C_{pf}=1575+1.708\times T$ $k_f=0.1388-0.0001881\times T$ $\mu_{log}=1.18616-0.01027\times T+5.31558\times10^{-5}\times T^2-3.06593\times10^{-7}\times T^3+1.12737\times10^{-9}\times T^4-2.18173\times10^{-12}\times T^5+1.68853\times10^{-15}\times T^6$ $\mu_f=10^{\mu_{log}}\times10^{-3}$
Therminol VP1 [41]	$\rho_f=1079-0.736\times T-0.0008826\times T^2+3.382\times10^{-6}\times T^3-6.472\times10^{-9}\times T^4$ $C_{pf}=1496+0.002521\times T+4.742\times10^{-6}\times T^2-2.503\times10^{-8}\times T^3+3.795\times10^{-11}\times T^4$ $k_f=0.1381-8.699\times10^{-5}\times T-1.734\times10^{-7}\times T^2$ $\mu_{log}=0.91282-0.01588\times T+1.04974\times10^{-4}\times T^2-5.09267\times10^{-7}\times T^3+1.49178\times10^{-9}\times T^4-2.33358\times10^{-12}\times T^5+1.49147\times10^{-15}\times T^6$ $\mu_f=10^{\mu_{log}}\times10^{-3}$
Xceltherm 600 [42]	$\rho_f=864-0.6073\times T$ $C_{pf}=1924+3.474\times T-0.0002094\times T^2$ $k_f=0.1377-8.087\times10^{-5}\times T$ $\mu_{log}=-0.79737-0.03404\times T+2.46372\times10^{-4}\times T^2-1.09169\times10^{-6}\times T^3+2.53174\times10^{-9}\times T^4-2.35632\times10^{-12}\times T^5$ $\mu_f=10^{\mu_{log}}$
Dowtherm J [43]	$\rho_f=878.8-0.7199\times T-0.000587\times T^2-4.785\times10^{-7}\times T^3+8.241\times10^{-9}\times T^4-2.967\times10^{-11}\times T^5$ $C_{pf}=1.768+0.00274\times T+5.581\times10^{-6}\times T^2+6.785\times10^{-9}\times T^3-1.43\times10^{-10}\times T^4+3.306\times10^{-13}\times T^5$ $k_f=0.1325-0.0002118\times T$ $\mu_{log}=0.09694-0.00768\times T+3.50003\times10^{-5}\times T^2-6.60814\times10^{-8}\times T^3-2.41532\times10^{-10}\times T^4+1.35078\times10^{-12}\times T^5-1.71781\times10^{-15}\times T^6$ $\mu_f=10^{\mu_{log}}$
Paratherm HR [44]	$\rho_f=954.4-0.5584\times T-0.0004887\times T^2$ $C_{pf}=1.899+0.001946\times T+2.016\times10^{-6}\times T^2-3.306\times10^{-9}\times T^3$ $k_f=0.1191-8.129\times10^{-5}\times T$ $\mu_{log}=2.01165-0.03383\times T+2.50434\times10^{-4}\times T^2-1.00925\times10^{-6}\times T^3+1.94427\times10^{-9}\times T^4-1.42236\times10^{-12}\times T^5$ $\mu_f=10^{\mu_{log}}$

$$\text{304L,} \quad k_{ab}=(0.013)T_{a_o-a_i}+15.2 \tag{46}$$

$$\text{316L,} \quad k_{ab}=(0.013)T_{a_o-a_i}+15.2 \tag{47}$$

$$\text{321H,} \quad k_{ab}=(0.0153)T_{a_o-a_i}+14.775 \tag{48}$$

HTFs have appreciable impact on the operation of PTSC and its efficiency. Different physical properties of an HTF required to run the model are ρ_f, C_{pf}, k_f, and μ_f. For an HTF, these properties vary with temperature which in turn alters the PTSC efficiency. To incorporate such variations, empirical relation is required for each physical property. So, data for each HTF is obtained from literature and using a curve fitting toolbox of MATLAB correlations are derived as depicted in Table 5.

To identify the best performing combination of design components, a combinatorial optimization was conducted using GA in MATLAB at two different temperatures. At 150 °C, the most efficient combination was found to be Dowtherm J+black nickel+304L with the PTSC efficiency of 76.89%. Next best combinations were Dowtherm J+Solel UVAC cermet a+304L (75.96%), Xceltherm 600+black nickel+304L (75.43%), and Paratherm HR+black nickel+304L (74.86%).

At 300 °C, many combinations were found to be evenly promising with matching efficiencies: Xceltherm 600+black nickel+304L (69.70%), Xceltherm 600+Solel UVAC cermet a+304L (69.68%), and Paratherm HR+Solel UVAC cermet a+304L (69.24%). The combination that was performing best at 150 °C was found to have an efficiency of 67.77% at 300 °C.

Results confirm that the performance of a particular combination is temperature dependent and a particular combination providing the best efficiency at certain temperature may lag at different temperatures. For instance, the combination Dowtherm J+black nickel+304L is performing best at 150 °C while lagging from others at 300 °C. Another aspect supporting the need for combinatorial optimization is that attractive properties cannot guarantee better performance. For example, at 150 °C, Dowtherm J has inferior thermal properties (C_{pf}, ρ_f, μ_f, and k_f) than Xceltherm 600, yet it promises better efficiency. It could also be noticed that black nickel with best absorptance value is a part of all the suggested combinations at 150 °C. Although it was found that at 300 °C Solel UVAC cermet a is a competitive prospect with Xceltherm 600 or even better with other HTFs.

Besides, it can be seen that the best suggested combinations at 300 °C are delivering similar efficiencies; the same situation is with second best combinations at 150 °C. Here, the choice of combination can be influenced by other factors such as the life of a component, strength and corrosive properties for absorber material, and cost, thus making the combinatorial optimization for PTSC, a more constrained and essential problem.

Overall, it is vital to analyze the performance of PTSC with this perspective also. An improvement of ~8% at 150 °C and ~6% at 300 °C in PTSC efficiency can be achieved compared to the aforementioned base case, supporting the significance of combinatorial optimization. Specifically, in IPH applications where the operating temperatures are almost fixed, this optimization can be really fruitful, as this combination of design components can best serve the application can be determined beforehand.

3. Geometric Optimization

As ascertained from section 4.1, varying the geometric parameters has a certain effect on the PTSC efficiency: positive or negative. So, by varying these parameters in a reasonable range, an optimal set providing improved efficiency can be obtained. The optimization process looks for those values of variables which optimize the objective function without violating the constraints. Here, an optimal set of geometric variables is required which maximizes the efficiency within the mentioned search space. As can be seen from Section 2, estimation of efficiency requires the evaluation of many nonlinear functions; traditional optimization methods fail to perform in such cases [45]. Since, nature has had great success in solving complicated problems, so nature-inspired algorithms are required for optimization purpose in such cases.

Hence, for finding an optimal set of geometric parameters, particle swarm optimization (PSO) is employed here. A MATLAB code is written that combines the PSO and model for optimization purpose. The current study makes efforts not only to estimate the optimal set of geometric parameters that maximizes efficiency but also check the effect of various operators of PSO on the current optimization problem. Thereby, the employed protocol checks and ensures that the geometric optimization problem of PTSC does not get trapped in a region of local maxima.

Geometric optimization is carried out for SEGS LS-2 collector comprising cermet coating with vacuum intact. To note the change in efficiency, a case from its experimental results is taken as a base with physical parameters such as inlet HTF temperature=151 °C, wind speed=3.70 m/s, T_s=22.4 °C, HTF flow rate=47.80 L/Min, DNI=968.2 W/m^2, and efficiency=70.90% at these conditions. The base values for geometric parameters and the ranges in which they are

Table 6. Geometric parameter(s) along with base values and search space

S. No.	Geometric parameter	Base value	Range (search space ±5%) Lower bound (LB) to Upper bound (UB)
1	D_{a_i}	0.066 m	0.063 m to 0.069 m
2	D_{e_i}	0.109 m	0.103 m to 0.114 m
3	f_{cl}	1.84 m	1.75 m to 1.93 m
4	l_{cl}	7.8 m	7.4 m to 8.2 m
5	w_{cl}	5 m	4.75 m to 5.25 m
6	D_{a_o}	0.070 m	D_{a_i}+0.004
7	D_{e_o}	0.115 m	D_{e_i}+0.006

varied for optimization are summarized in Table 6.

3-1. Particle Swarm Optimization (PSO)

PSO imitates the social and cooperative behavior displayed by various natural species (birds, fishes, etc.) and was introduced by Kennedy and Eberhart [46]. It has various advantages: easy implementation, high convergence, and less dependency on initial val-

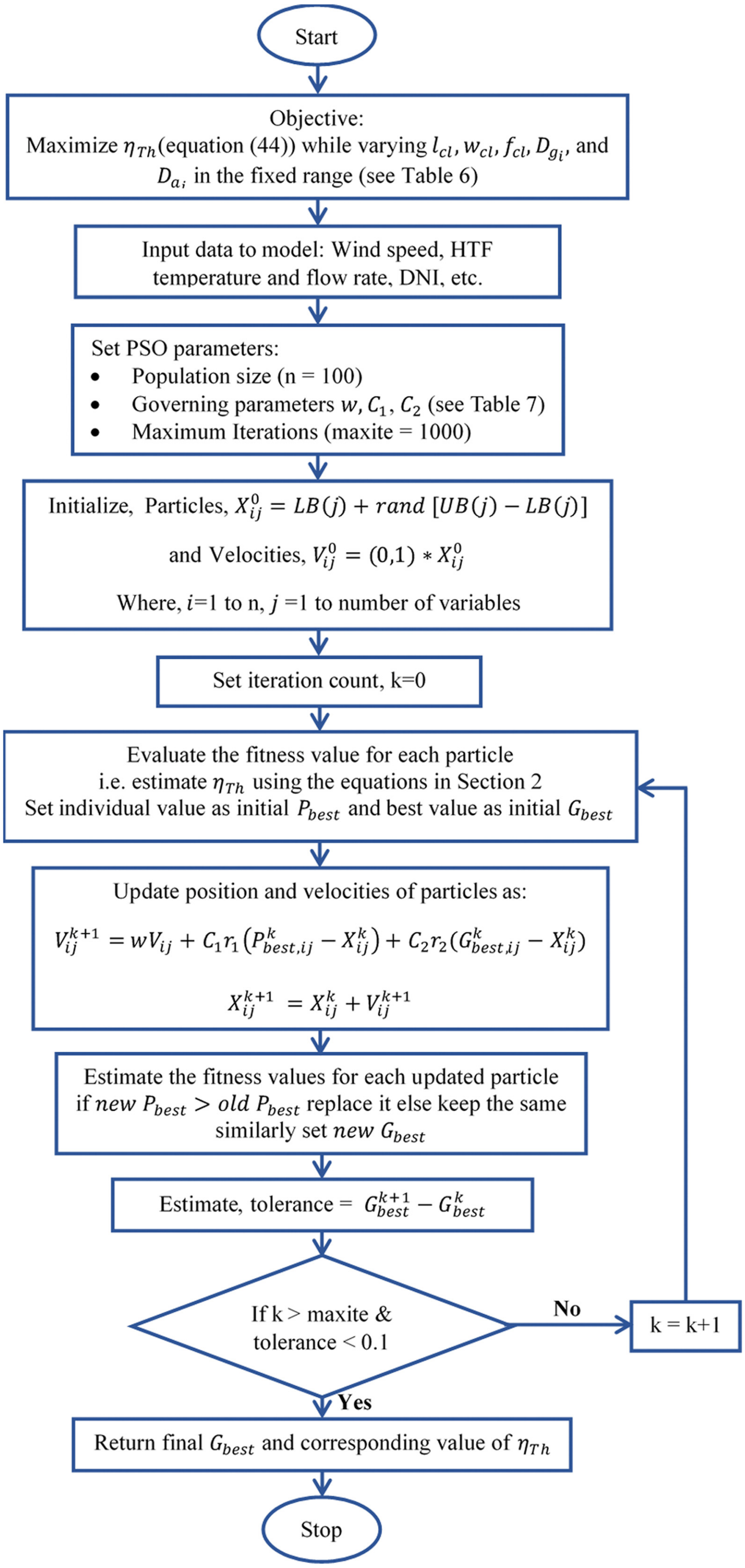

Fig. 9. Optimization procedure to determine the optimal set of geometric parameters using PSO.

Table 7. Various PSO operators and corresponding optimal values of geometric parameters

S. No.	PSO operators			Optimal values in ±5% Search space					η
	w	C_1	C_2	D_{a_i}	D_{e_i}	f_{cl}	w_{cl}	l_{cl}	
1	Linearly decreasing from 0.9 to 0.4	1.49618	1.49618	0.0644	0.1033	1.7764	4.7538	7.8887	74.09
2	Linearly decreasing from 0.9 to 0.4	2	2	0.0651	0.1107	1.7790	4.7508	7.8496	74.05
3	Constant=0.7298	1.49618	1.49618	0.0634	0.1078	1.7813	4.7631	8.1637	74.23
4	Constant=0.7298	2	2	0.0631	0.1043	1.7639	4.7576	8.1522	74.35

ues [47]. It constitutes a base population known as a swarm, which represents the set of potential solutions. Each individual within the swarm is known as particle and is a potential solution to a problem. Particles move around in a search space and interact with one another while learning from their own experiences (P_{best}) and others' experiences (G_{best}). Gradually, the population members move towards the better region of the problem space. Fig. 9 displays the detailed optimization procedure followed in this study to estimate the optimal geometry using PSO.

Here, w is known as inertia weight factor, C_1 and C_2 are acceleration constants, r_1 and r_2 are the uniformly generated random numbers in the range [0,1]. w controls the exploration and exploitation, $w \geq 1$ increases the velocities over time and diverges the swarm and vice versa when $w<0$. A value of $0<w<1$ is suggested for good convergence and is influenced by C_1, C_2. The importance of P_{best} is affected by C_1, while C_2 controls the impact of G_{best}. If $C_1>0$ and $C_2=0$, particles tend to get trapped in local search and If $C_1=0$ and $C_2>0$, the entire swarm gets attracted towards a single point [48]. Thus, it becomes important to check and choose these parameters according to the problem at hand.

Several adjustments in parameters are suggested by researchers; few matured ones are tested for our problem. Conventionally, $C_1= C_1=2$ and $0<w<1$ are used as the parameters, but it is empirically tested that $w=0.7298$ and $C_1=C_1=1.49618$ provides good convergence behavior [49]. Eberhart and Shi have suggested that the value of w linearly decreasing from 0.9 to 0.4 during a run provides a better performance in numerous applications [50]. Considering these, four different sets of PSO parameters shown in Table 7 were used for optimization; corresponding optimal sets of geometric parameters are also displayed.

It can be perceived that with the optimal sets obtained through PSO, reasonable improvement in efficiency (from 70.90% to ~74%) can be achieved and is similar for all the parameter sets. Thus, the PSO utilized here for geometric optimization can be used with any of the mentioned parameters. Although, it could be a possibility that with geometric and physical parameters considered here, its behavior is stable and might get changed when applied for a different setup. So, it is advisable to use w linearly decreasing from 0.9 to 0.4, which gradually takes the search from exploration to exploitation, along with any of the indicated values for $C_1=C_1$.

A decent improvement in efficiency advocates that it is good to make optimal improvements in the geometric parameters of PTSC. If such analysis is done before manufacturing PTSC modules for a specific application, considerable benefits can be attained. Especially in IPH applications, such improved efficiency means an early recovery of the investment, thus attracting more share of PTSCs in industries.

CONCLUSIONS

An analytical model of parabolic trough solar collector (PTSC) was formulated for analyzing its performance on various factors. The model was simulated for three different PTSC setups: SEGS LS-2, IST PTSC, and HTF test bench. Obtained simulation results were compared with experimental results from the mentioned setups and the model was found to be very reliable, thereby approving its usage for analysis and optimization purposes for PTSC.

Sensitivity analysis pertaining to variation in the combination of design components revealed the need for combinatorial optimization for PTSC. It was established that PTSC involves many interacting factors that affect its efficiency and solely good properties of the design components cannot guarantee better performance. Moreover, it was revealed that the performance of a particular combination of components is temperature-dependent. Consequently, combinatorial optimization was carried out using genetic algorithm (GA) for six solar selective absorber coatings (SSACs), three absorber materials, and five heat transfer fluids (HTFs), leading to 90 different combinations. Notable improvements of ~8% at 150 °C and ~6% at 300 °C in the efficiency were observed. At 150 °C, the combination yielding the highest efficiency was found to be Dowtherm J+black nickel+304L. At 300 °C, three different combinations as Xceltherm 600+black nickel+304L, Xceltherm 600+Solel UVAC cermet a+304L, and Paratherm HR+Solel UVAC cermet a+304L were found to deliver the maximum but approximately same efficiency. For such a case, cost or any other factor can become a deciding factor in choosing the best combination.

The current work also pursued a detailed sensitivity analysis demonstrating the effect of variation in geometric parameters of PTSC over its efficiency. Both positive and negative impacts on the efficiency were noted while varying the geometric parameters like l_{cl}, w_{cl}, f_{cl}, D_{e_i} and D_{a_i}. It is identified that an optimal set providing improved efficiency can be obtained by varying these parameters in a reasonable range. To determine such an optimal set, geometric optimization was conducted using particle swarm optimization (PSO). In addition, the effect of various operators of PSO (w, C_1, C_2) on the current optimization problem was also reported. It was found that the current problem is sparsely affected by PSO operators, and efficiency improvement of ≥3% is noticed by only ±5% variation in geometry.

Altogether, it turns out that PTSCs have many parameters in terms of design components and geometric specifications that affect their performance. If it is to be utilized for IPH applications that have specific needs, i.e., operating temperatures and working medium (air, steam, fluid, etc.) are generally fixed. It becomes crucial to employ a PTSC that has an optimal set of components and dimensions, delivering the maximum output. This can be recognized beforehand by utilizing the optimization approaches outlined in this paper. Besides SSACs, absorber material, and HTFs considered here, other parameters can also be included, and a number of options for each of them can also be increased depending upon the problem. The optimization methods discussed here are applicable for any number of combinations of design components and any PTSC setup.

In this study, combinatorial optimization explored the best possible combination of design components for SEGS LS-2 collector with a fixed geometry only. Although, it was found that slight variations in geometry can also improve thermal efficiency. It raises the possibility that each of the 90 combinations explored here may have their corresponding optimal geometry. This prospect was not explored here and is a potential limitation of this study.

ACKNOWLEDGEMENT

The first author is grateful to the Ministry of Human Resource Development (MHRD), India for providing financial support in the form of Senior Research Fellowship.

NOMENCLATURE

A : area [m^2]
Ac : accommodation coefficient [-]
b : interaction coefficient [-]
C_p : specific heat capacity [J/kg °C]
D : diameter [m]
E_θ : end loss [-]
fr : friction factor [-]
f_{cl} : focal length of PTC [m]
h : convective heat transfer coefficient [W/m^2 °C]
k : thermal conductivity [W/m °C]
K_θ : incident angle modifier [-]
l_{cl} : length of the collector [m]
l_{hce} : length of HCE [m]
L : length [m]
Nu : Nusselt number [-]
P : Perimeter [m]
P_{ga} : pressure of annulus gas [mmHg]
Pr : Prandtl number [-]
Q : heat flux per unit length [W/m]
Ra : Rayleigh number [-]
Re : Reynolds number [-]
T : temperature [°C]
w_{cl} : width of the collector [m]

Greek Letters

α : absorptance [-]
γ : ratio of specific heats of annulus gas [-]
γ_{in} : intercept factor [-]
δ : molecular diameter of annulus gas [-]
ε : emissivity [-]
η_{O-ab} : optical efficiency at absorber surface [-]
η_{O-e} : optical efficiency at glass envelope [-]
θ : angle of incidence [°]
λ : mean-free-path between collisions of a molecule [m]
μ : viscosity [Pa·s]
ξ : perpendicular distance between axis of annulus surfaces [m]
ρ : density [kg/m^3]
σ : Stefan-Boltzmann constant [=5.67×10^{-8} W/m^{2}K^4]
τ : transmittance [-]

Subscripts

a_i : inner surface of absorber
a_o : outer surface of absorber
a_i-f : between inner surface of absorber and heat transfer fluid
a_o-a_i : between outer and inner surface of absorber
a_o-e_i : between outer surface of absorber and inner surface of glass envelope
ab : absorber
Ab : absorbed solar energy
an_Cond : heat transfer in annulus via conduction
an_Conv : heat transfer in annulus via convection
Brac : support bracket
cl : collector
Conv : convection
Cond : conduction
eff : effective
F : forced convection
e : glass envelope
e_i : inner surface of glass envelope
e_o : outer surface of glass envelope
e_i-e_o : between inner and outer surface of glass envelope
e_o-s : between outer surface of glass envelope and surroundings
e_o-sky : between outer surface of glass envelope and sky
f : heat transfer fluid
g : gas in annulus
hce : heat collector element
l : laminar flow
N : natural convection
Rad : radiation
s : surroundings/ambient
Sol : solar energy
t : turbulent flow
ug : useful heat gained

Abbreviations

DNI : direct normal irradiation
GA : genetic algorithm
HCE : heat collector element
HTF : heat transfer fluid
IST : industrial solar technology
IPH : industrial process heat
LS-2 : Luz system 2nd generation
PTSC : parabolic trough solar collector
PSA : plataforma solar de almeria
PSO : particle swarm optimization

RMSE : root mean square error
SEGS : solar electric generating systems
SNL : sandia national laboratory
SSAC : solar selective absorber coating

REFERENCES

1. V. K. Jebasingh and G. M. J. Herbert, *Renew. Sustain. Energy Rev.*, **54**, 1085 (2016).
2. A. Goel, G. Manik and R. Mahadeva, in *Advances in intelligent systems and computing*, Pant M., Sharma T., Verma O., Singla R. (Eds.), Springer, Singapore (2020).
3. S. Kalogirou, *Appl. Energy*, **76**, 337 (2003).
4. R. Silva, C. Francisco Javier and M. Pérez-garcía, *Energy Procedia.*, **48**, 1210 (2014).
5. O. P. Verma, G. Manik and T. H. Mohammed, *Korean J. Chem. Eng.*, **34**, 2570 (2017).
6. A. Fernández-García, E. Zarza, L. Valenzuela and M. Pérez, *Renew. Sustain. Energy Rev.*, **14**, 1695 (2010).
7. W. Ajbar, A. Parrales, U. Cruz-Jacobo, R. A. Conde-Gutiérrez, A. Bassam, O. A. Jaramillo and J. A. Hernández, *Appl. Therm. Eng.*, **189**, 116651 (2021).
8. H. Habibi, M. Zoghi, A. Chitsaz and M. Shamsaiee, *Appl. Therm. Eng.*, **180**, 115827 (2020).
9. Q. Liu, M. Yang, J. Lei, H. Jin, Z. Gao and Y. Wang, *Sol. Energy*, **86**, 1973 (2012).
10. P. Mohammad Zadeh, T. Sokhansefat, A. B. Kasaeian, F. Kowsary and A. Akbarzadeh, *Energy*, **82**, 857 (2015).
11. T. E. Boukelia, O. Arslan and M. S. Mecibah, *Appl. Therm. Eng.*, **107**, 1210 (2016).
12. R. Silva, M. Berenguel, M. Pérez and A. Fernández-Garcia, *Appl. Energy*, **113**, 603 (2014).
13. W. Wang, M. Li, R. H. E. Hassanien, M. E. Ji and Z. Feng, *Int. J. Green Energy*, **14**, 819 (2017).
14. O. May Tzuc, A. Bassam, M. A. Escalante Soberanis, E. Venegas-Reyes, O. A. Jaramillo, L. J. Ricalde, E. E. Ordoñez and Y. El Hamzaoui, *J. Renew. Sustain. Energy*, **9**, 1 (2017).
15. E. Bellos and C. Tzivanidis, *Energy*, **149**, 47 (2018).
16. H. Hoseinzadeh, A. Kasaeian and M. B. Shafii, *Energy Sci. Eng.*, **7**, 2950 (2019).
17. M. A. Ehyaei, A. Ahmadi, M. El Haj Assad and T. Salameh, *J. Clean. Prod.*, **234**, 285 (2019).
18. Z. D. Cheng, Y. L. He, B. C. Du, K. Wang and Q. Liang, *Appl. Energy*, **148**, 282 (2015).
19. R. López-Martín and L. Valenzuela, *Case Stud. Therm. Eng.*, **12**, 414 (2018).
20. R. Forristall, Heat Transfer Analysis and Modeling of a Parabolic Trough Solar Receiver Implemented in Engineering Equation Solver, NREL/TP-550-34169 (2003).
21. J. A. Duffie and W. A. Beckman, *Solar engineering of thermal processes*, 4th Ed., John Wiley & Sons, Inc. (2013).
22. V. E. Dudley, G. J. Kolb, M. Sloan and D. Kearney, Test results - SEGS LS2 collector. Sandia National Laboratories (1994).
23. V. E. Dudley, L. R. Evans and C. W. Matthews, Test results, Industrial Solar Technology parabolic trough solar collector (1995).
24. L. Valenzuela, R. López-Martín and E. Zarza, *Energy*, **70**, 456 (2014).
25. F. Lippke, Simulation of the part-load behaviour of a 30 MW SEGS plant (1995).
26. F. Incropera and D. Dewitt, *Fundamentals of heat and mass transfer*, 6th Ed., John Wiley & Sons (2006).
27. Y. A. Cengel and A. J. Ghajar, *Heat and mass transfer*, 5th Ed., McGraw-Hill Education (2015).
28. W. C. Swinbank, *Q. J. R. Meteorol. Soc.*, **89**, 339 (1963).
29. W. M. Rohsenow and J. R. Hartnett, *Handbook of heat transfer*, 3rd Ed., McGraw-Hill Education (1999).
30. V. Gnielinski, *Int. J. Heat Mass Transf.*, **63**, 134 (2013).
31. A. C. Ratzel, C. E. Hickox and D. K. Gartling, *J. Heat Transf. Trans ASME*, **101**, 108 (1979).
32. T. H. Kuehn and R. J. Goldstein, *Int. J. Heat Mass Transf.*, **19**, 1127 (1976).
33. S. W. Churchill and R. Usagi, *AIChE J.*, **18**, 1121 (1972).
34. V. T. Morgan, *Adv. Heat Transf.*, **11**, 199 (1975).
35. H. Yılmaz and M. S. Söylemez, *Energy Convers. Manag.*, **88**, 768 (2014).
36. R. V. Padilla, *Simplified methodology for designing parabolic trough solar power plants*, University of South Florida (2011).
37. R. Aguilar, L. Valenzuela, A. L. Avila-Marin and P. L. Garcia-Ybarra, *Energy Convers. Manag.*, **196**, 807 (2019).
38. S. N. Sivanandam and S. N. Deepa, *Principles of soft computing*, Wiley India Pvt. Ltd, New Delhi (2017).
39. J. J. Valencia and P. N. Quested, Thermophysical Properties, in: ASM Handb., ASM international, 468 (2008).
40. Dow Corning Corporation, SYLTHERM 800 Heat Transfer Fluid: Product Technical Data, 1997. http://www.dow.com/heattrans.
41. Eastman, Therminol VP-1, Technical Bulletin TF9141, 2019. https://www.eastman.com/Literature_Center/T/TF9141.pdf.
42. HEAT TRANSFER FLUIDS XCELTHERM ® 600 - Engineering Properties (2015).
43. H. T. Fluid, DOWTHERM J Heat Transfer Fluid, 1 (1977).
44. S. Heat, T. Conductivity and V. Pressure, PARATHERM™ HR SYNTHETIC-AROMATIC HEAT, 1 (2020).
45. A. Hojjati, M. Monadi, A. Faridhosseini and M. Mohammadi, *J. Hydrol. Hydromechanics*, **66**, 323 (2018).
46. J. Kennedy and R. Eberhart, Particle swarm optimization, in: Proc. ICNN'95 - Int. Conf. Neural Networks, IEEE, n.d.: pp. 1942-1948. https://doi.org/10.1109/ICNN.1995.488968.
47. M. Kumar, S. C. Sharma, S. Goel, S. K. Mishra and A. Husain, *Neural Comput. Appl.*, **32**, 18285 (2020).
48. Y. Shi, Russell Eberhart, A modified particle swarm optimizer algorithm, 2007 8th Int. Conf. Electron. Meas. Instruments, ICEMI. (2007) 2675-2679. https://doi.org/10.1109/ICEMI.2007.4350772.
49. F. Van Den Bergh and A. P. Engelbrecht, *Inf. Sci. (Ny)*, **176**, 937 (2006).
50. R. C. Eberhart and Y. Shi, Comparing inertia weights and constriction factors in particle swarm optimization, Proc. 2000 Congr. Evol. Comput. CEC 2000. 1 (2000) 84-88. https://doi.org/10.1109/CEC.2000.870279.

APPENDIX

Table A1. Experimental data for SEGS LS-2 collector comprising cermet SSAC with vacuum in annulus alongside the comparison between experimentally noted efficiency and model estimations

DNI (w/m^2)	Wind (m/s)	Flow rate (L/min)	T_{amb} (°C)	T_{in} (°C)	Efficiency	
					SNL tests	Proposed model
933.7	2.60	47.70	21.2	102.2	72.51	70.88
968.2	3.70	47.80	22.4	151.00	70.90	70.22
982.3	2.50	49.10	24.3	197.50	70.17	69.91
909.5	3.30	54.70	26.2	250.70	70.25	68.96
937.9	1.00	55.50	28.8	297.80	67.98	68.40
880.6	2.90	55.60	27.5	299.00	68.92	67.40
903.2	4.20	56.30	31.1	355.90	63.82	63.64
920.9	2.60	56.80	29.5	379.50	62.34	63.03
RMSE						**0.990**

Table A2. Experimental data for SEGS LS-2 collector comprising cermet SSAC with air in annulus alongside the comparison between experimentally noted efficiency and model estimations

DNI (w/m^2)	Wind (m/s)	Flow rate (L/min)	T_{amb} (°C)	T_{in} (°C)	Efficiency	
					SNL tests	Proposed model
813.1	3.6	50.3	25.8	101.2	71.56	70.14
858.4	3.1	52.9	27.6	154.3	69.20	70.58
878.7	3.1	54.6	28.6	202.4	67.10	68.21
896.4	0.9	55.2	30.0	250.7	65.50	66.38
889.7	2.8	55.3	28.6	251.1	66.61	65.83
906.7	0.0	55.4	31.7	299.5	62.58	61.19
874.1	4.0	56.2	28.7	344.9	59.60	58.86
870.4	0.6	56.1	29.1	345.5	59.40	58.84
879.5	1.8	55.4	27.4	348.9	58.52	58.13
898.6	2.8	56.2	29.7	376.6	56.54	55.69
RMSE						**1.010**

Table A3. Experimental data for SEGS LS-2 collector comprising black chrome SSAC with vacuum in annulus alongside the comparison between experimentally noted efficiency and model estimations

DNI (w/m^2)	Wind (m/s)	Flow rate (L/min)	T_{amb} (°C)	T_{in} (°C)	Efficiency	
					SNL tests	Proposed model
744.6	1.1	50.7	−5	100.8	72.47	72.04
839.8	1.1	50.6	3.6	103.4	73.56	71.49
902	0	52.1	6.4	154	72.1	71.63
871.8	4	53.2	1.6	201.5	69.69	69.15
900.7	1.3	54	0.2	201.6	69.91	70.06
882.7	2.1	54.8	−3.1	253.3	69.58	68.66
884.6	3	54.9	2.6	303.1	65.36	64.88
921.5	0	56	−0.7	349.6	61.49	62.90
928.4	2.4	56.1	−0.9	379.6	57.7	59.39
RMSE						**1.045**

Table A4. Experimental data for SEGS LS-2 collector comprising black chrome SSAC with air in annulus alongside the comparison between experimentally noted efficiency and model estimations

DNI (w/m^2)	Wind (m/s)	Flow rate (L/min)	T_{amb} (°C)	T_{in} (°C)	Efficiency	
					SNL tests	Proposed model
755.0	5.5	50.3	−1.0	101.9	69.07	70.47
902.6	1.7	52.1	5.1	154.2	67.88	68.69
850.9	4.7	54.3	−0.6	203.2	64.14	63.94
909.6	1.2	55.0	1.3	251.8	63.32	64.07
899.7	4.4	56.2	0.5	301.6	60.08	60.09
908.1	5.9	55.6	5.9	350.2	56.17	55.72
919.5	1.4	56.2	0.1	379.7	53.71	52.32
RMSE						**0.874**

Table A5. Experimental data for IST PTSC collector comprising black chrome SSAC with air in annulus alongside the comparison between experimentally noted efficiency and model estimations

DNI (w/m^2)	Wind (m/s)	Flow rate (L/min)	T_{amb} (°C)	T_{in} (°C)	Efficiency	
					SNL tests	Proposed model
995.5	2.9	48.2	11.8	100.20	67.01	67.97
1,005.7	3.9	50.4	14.1	151.38	64.26	63.43
875.5	1.8	51.0	16.1	200.65	60.35	59.55
927.2	3.7	51.9	10.2	251.34	54.82	54.23
994.9	4.1	52.5	14.0	297.75	50.04	49.51
977.1	4.4	53.0	16.0	338.16	43.27	43.77
RMSE						**0.722**

Table A6. Experimental data for IST PTSC collector comprising black nickel SSAC with air in annulus alongside the comparison between experimentally noted efficiency and model estimations

DNI (w/m^2)	Wind (m/s)	Flow rate (L/min)	T_{amb} (°C)	T_{in} (°C)	Efficiency	
					SNL tests	Proposed model
907.5	2.0	44.3	5.3	61.36	73.44	72.79
957.9	2.3	48.0	6.7	98.82	70.95	69.55
966.7	5.6	50.2	9.7	150.82	67.43	68.31
939.8	5.8	51.7	10.2	200.93	63.97	62.61
902.5	5.1	52.3	10.8	249.00	59.29	59.18
904.4	2.6	52.8	10.1	298.15	54.40	53.82
RMSE						**0.944**

Table A7. Experimental data for IST PTSC HTF test bench alongside the comparison between experimentally noted efficiency and model estimations

θ (°)	DNI (w/m^2)	Flow rate (m^3/h)	T_{amb} (°C)	T_{in} (°C)	Efficiency	
					Tests at PSA labs	Proposed model
18.4	894	14.74	28.9	250.6	72.7	72.19
16.1	943	14.97	34.1	284.9	72.7	72.28
26.9	798	14.98	25.6	286	69.8	68.07
9.2	927	15.01	33.8	316.5	71.8	72.84
16.1	911	15.03	35.1	316.9	71.8	71.48
21.3	833	15.03	26.4	316.5	69.6	69.04
16	875	15.04	27.7	316.7	70.9	71.69
30.7	904	15.2	24.6	334.8	67.9	66.47
19.5	918	15.13	25.2	334.8	70.6	69.94
12	919	15.4	32.9	334.5	71.1	72.61
RMSE						**1.015**